

Rock magnetism of a loess-palaeosol sequence from the western Black Sea shore (Romania)

Cristian Necula, Daniela Dimofte and Cristian Panaiotu

University of Bucharest, Paleomagnetic Laboratory, 010041 Bucharest, Romania. E-mail: cristian.panaiotu@gmail.com

Accepted 2015 June 9. Received 2015 June 8; in original form 2015 March 6

SUMMARY

The Lower Danube Basin is one of the most important loess regions from Europe, which have provided excellent archives for long-term high-resolution palaeoclimate studies. The aim of this paper is to derive new information on the Middle–Late Pleistocene palaeoenvironment from a high resolution multiproxy assessment of the iron mineralogical composition at the Costinești loess-palaeosol sequence located on the western Black Sea shore. It is the easternmost loess section in the Romanian loess region studied and its distinct pattern of the proxy records can be used to correlate the lower Danube loess to other key sites of the Moldavia and Ukraine loess regions. To investigate the climatic control on soft and hard ferromagnetic minerals we used several types of rock magnetic properties: magnetic susceptibility and its frequency dependence, anhysteretic remanent magnetization, isothermal remanent magnetization, hysteresis properties and FORC distributions, an unmixing model for isothermal remanent magnetization curves and high field (up to 8 T) isothermal remanence measurements. Our results show that the palaeosol horizons, formed during interglacials and climatically more favored periods of the Pleistocene, experienced pedogenic alteration, resulting in high amounts of superparamagnetic, single domain and pseudosingle domain magnetite/maghemite grains and hematite. The loess layers, formed during glacial periods, are mainly dominated by multidomain and/or pseudosingle domain oxidized magnetite and some hematite, all probably of aeolian origin. Goethite contribution is probably minor and constant both in loess and palaeosol horizons. We review the correlation of the loess sections from the lower Danube basin concluding that the new results can be interpreted as a support for the transition of a Mediterranean type climate to a steppe type climate in the last two interglacial periods in the western Black Sea. Because the pattern of magnetic susceptibility data from the lower Danube basin is changing relative fast with distance from the Black Sea shore, it probably reflects the local influence of the Black Sea on continental scale climatic oscillations during the last 600 ka. The values of background magnetic susceptibility of the Romanian loess-palaeosol sections indicate that the main source area of the dust changed during this climatic transition. Our analysis also shows that the age of the loess-palaeosol sections from the Eastern European low lands (Moldavia and Ukraine) must be revised to be in agreement with the chronostratigraphy of the sections from the Lower Danube Basin loess area.

Key words: Environmental magnetism; Rock and mineral magnetism; Europe.

1 INTRODUCTION

Southeastern Europe is one of the important European loess areas (Haase *et al.* 2007). The Middle and Lower Danube Basins are among the five important loess areas defined by Smalley *et al.* (2009) along the Danube River. In particular, the Lower Danube Basin loess area is important, because it makes the connection with the loess areas of the Eastern European lowland (Haase *et al.* 2007). Palaeoclimatic studies performed on several well-preserved

European loess-palaeosol deposits located along the Danube River have shown that rock magnetic palaeoenvironmental proxies are similar to those of the loess sections from the Chinese Loess Plateau and can be correlated with marine records of global ice volume (e.g. Fitzsimmons *et al.* 2012 and references there in; Marković *et al.* 2012). Rock magnetic properties of several loess deposits from Serbia, Bulgaria and Romania revealed magnetite and/or maghemite as the dominant magnetic carrier of palaeoclimatic information (e.g. Jordanova & Petersen 1999; Panaiotu *et al.* 2001;

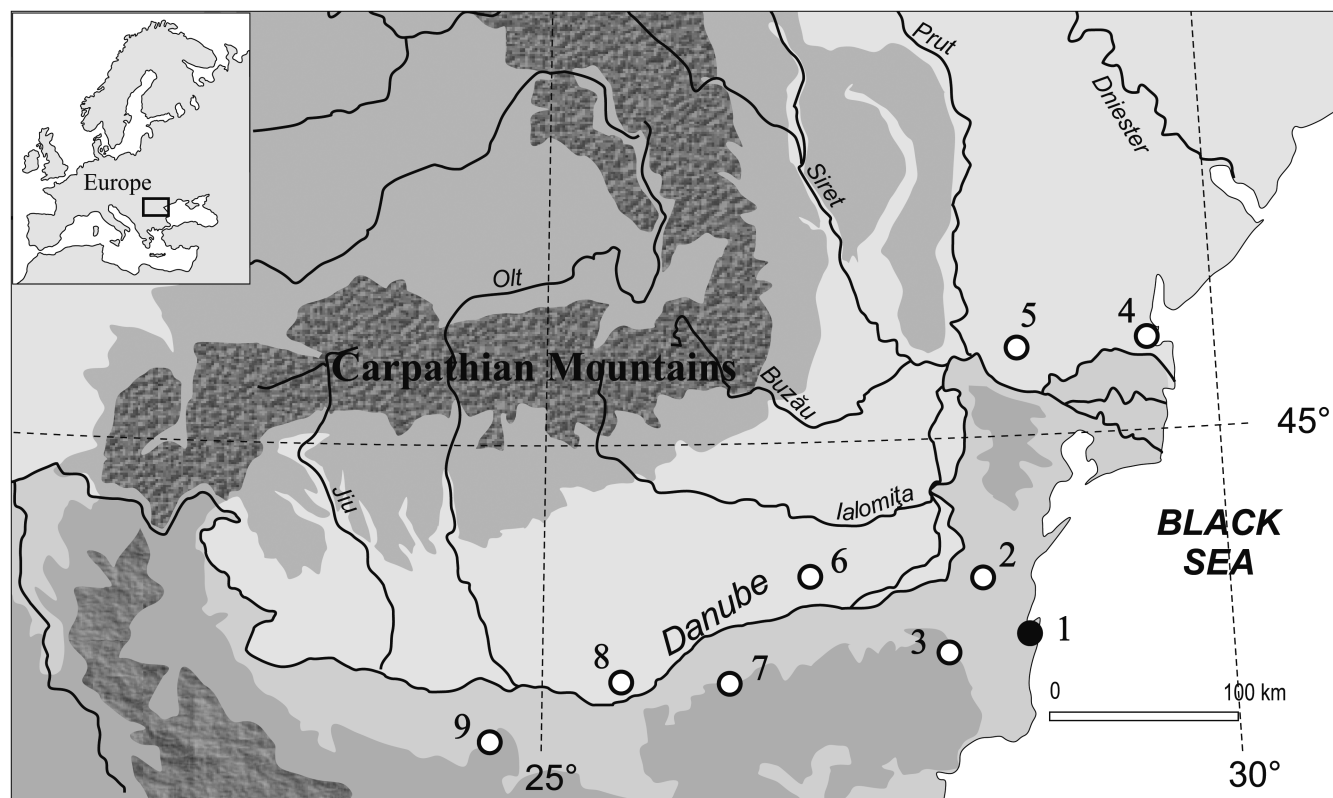


Figure 1. Sketch map of the lower Danube basin showing the locations of the loess-palaeosol sections discussed in the text: 1. Costinești (full circle, Romania); 2. Mircea Vodă (Romania); 3. Koriten (Bulgaria); 4. Primorskoje (Ukraine); 5. Nova Etulyia (Moldavia); 6. Mostiștea (Romania); 7. Viatovo (Bulgaria); 8. Zimnicea (Romania); 9. Lubenovo (Bulgaria).

Jordanova *et al.* 2007; Buggle *et al.* 2009, 2014; Marković *et al.* 2009, 2011; Necula *et al.* 2013). Recent studies have shown that in the Serbian, Bulgarian and Romanian loess-palaeosol deposits the antiferromagnetic signal is also enhanced in palaeosols proving that the palaeosols experienced a higher degree of weathering than loess units (Jordanova *et al.* 2011; Buggle *et al.* 2014; Lukic *et al.* 2014). However, in the abovementioned studies the Romanian loess is represented only by one section (Mircea Vodă, Fig. 1) and the evidence about the presence of hematite and goethite is primarily based on the application of diffuse reflectance spectroscopy (DRS) and colour determination employing the Munsell color chart (Buggle *et al.* 2014).

This study presents the first detailed rock magnetic investigation of a loess-palaeosol section located on the Romanian shore of the Black Sea. Our aim was to establish the contribution of both soft (magnetite/maghemite) and hard (hematite and goethite) magnetic minerals to the magnetic mineralogy of the bulk samples and to obtain information concerning the magnetic granulometry using room-temperature magnetic measurements. In addition, the nearby Mircea Voda loess-palaeosol section (Buggle *et al.* 2009; Necula *et al.* 2013) was also investigated for antiferromagnetic mineralogy using magnetic measurements. This will allow the comparison with the DRS derived antiferromagnetic contribution obtained for this section by Buggle *et al.* (2014). These results will provide new insights about the relationship between iron oxide mineralogy and palaeoclimate evolution in the Romanian loess. Based on the new data we propose a new correlation of the Lower Danube Basin loess deposits.

2 STUDY AREA

The studied loess-palaeosol section is located on the Black Sea shore ($43^{\circ}57.304'N$, $28^{\circ}38.428'E$; Fig. S1), in the Costinești village, about 70 km SE from the Danube river and around 50 km from the Mircea Vodă loess-palaeosol section (Fig. 1, S5). It contains five loess layers (L1–L5), the recent soil (S0) and five palaeosols (S1–S5). The maximum thickness is around 12.5 m. The recent soil S0 and palaeosols S1 and S2 are steppe soils, whereas S3–S5 are brown-reddish forest soils (Conea 1970). According to Buggle *et al.* (2013, 2014) elsewhere in the Dobrogea plateau (the Mircea Vodă section), the palaeosols S1 and S2 are fossil steppe soils, the palaeosols S3 and S4 are fossil forest steppe soils and palaeosol S5 is fossil cambisol. The Quaternary deposit is developed on Sarmatian limestone (e.g. Constantin *et al.* 2014). The same sequence of loess and palaeosols can be followed along the Black Sea shore for 7 km toward the north, and to the south for more than 3 km, near the border with Bulgaria. Images of these loess deposits are presented in the Figs S1–S4. It must be pointed out that in the other locations below the palaeosol S5 there is thin loess layer (<0.5 m) followed by a 1.5-m-thick red palaeosol. The same sequence of palaeosols can be found along the coast towards the south in Bulgaria (Avramov *et al.* 2006).

A chronostratigraphy of these deposits was established using infrared stimulated luminescence (IRSL) on feldspar by Balescu *et al.* (2003) and optically stimulated luminescence (OSL) by Constantin *et al.* (2014). These studies have shown that the first three loess layers were formed during marine isotope stage (MIS) 2–4, 6

and 8, and the corresponding palaeosols S1, S2 and S3 during MIS 5, 7 and 9. A magnetic time depth-model based on the correlation of magnetic susceptibility with the stack of 57 globally distributed benthic $\delta^{18}\text{O}$ records (Lisiecki & Raymo 2005) was in agreement with these luminescence ages and indicated that palaeosols S4 and S5 can be correlated with MIS 11 and MIS 13–15, respectively (Constantin *et al.* 2014).

3 METHODS

The Costinești sequence was cleaned and sampled at around 5-cm-interval in plastic bags (245 samples). In the laboratory samples were packed in 11 cm³ plastic cylinders for bulk magnetic susceptibility measurements. All magnetic measurements were performed at the Palaeomagnetic Laboratory, University of Bucharest.

Magnetic susceptibility (χ) was measured using an AGICO MFK1A Kappabridge (χ_{lf} at 976 Hz and χ_{hf} at 15 616 Hz). Frequency dependent magnetic susceptibility was defined by χ_{fd} (per cent) = $100(\chi_{\text{lf}} - \chi_{\text{hf}})/\chi_{\text{lf}}$ (Dearing *et al.* 1996). In order to compare background magnetic susceptibility values of the Romanian loess-palaeosol sequences, frequency dependence of magnetic susceptibility of the Costinești and Mircea Vodă samples was also measured using a MS2B Bartington Magnetic Susceptibility System (χ_{lf} at 465 Hz and χ_{hf} at 4650 Hz). This was necessary to avoid the calibration differences between the AGICO Kappabridge and MS2B Bartington Magnetic Susceptibility System (Sagnotti *et al.* 2003; Fukuma & Torii 2011), because the Mostiștea section was measured using the MS2B Bartington Magnetic Susceptibility System (Panaiotu *et al.* 2001).

Anhyseretic remanent magnetization (ARM) was induced using a Magnon International AF Demagnetizer in a peak alternating field (AF) of 100 mT and a steady field of 0.05 mT. χ_{ARM} was then obtained by dividing the mass-normalized ARM values by the bias field applied during ARM acquisition. An isothermal remanent magnetization ($\text{IRM}_{2\text{T}}$) was induced using a Magnon International pulse magnetizer in a field of 2 T. All remanences were measured using an AGICO JR5 spinner magnetometer.

Backfield remanent moment and direct moment curves were measured on 132 samples (around 10 cm sampling interval) using a Vibrating Sample Magnetometer model 3900 (PMC MicroMag). Samples were first saturated at 1 T and then the field was reversed and nonlinearly incremented until -1 T in 30 steps. The saturation magnetization (M_s), saturation remanent magnetization (M_{rs}), coercive force (B_c) and coercivity of remanence (B_{cr}) were calculated after correction for the paramagnetic contribution. The S ratio was calculated as $S = -\text{IRM}_{-300\text{mT}}/\text{IRM}_{1\text{T}}$ (e.g. Verosub & Roberts 1995; Quinton *et al.* 2011).

To interpret backfield demagnetization curves, we used the IRM unmixing algorithm of Heslop and Dillon (2007). For this purpose, the mass-normalized backfield data were rescaled (division by a factor of 2), reversed and inverted in order to simulate IRM acquisition curves (Heslop & Dillon 2007). The algorithm requires all backfield acquisition curves to be measured using an identical sequence of fields. Therefore we used linear interpolation to fix all the curves to the same sequence of fields. The unmixing algorithm assumes that all IRM curves can be explained by a linear mixture of a small number of end-members (EMs). The estimation of the number of end-EMs included in the unmixing model was based on the calculation of the coefficient of determination, R^2 , versus the number of EMs through principal component analysis (Heslop & Dillon 2007).

Representative samples of loess and palaeosol horizons were measured to produce first-order reversal curve (FORC) distributions. For each sample 111 first-order reversal curves were measured using a saturating field of 1 T. Both loess and palaeosol samples were measured with a field increment of 1.73 mT (B_u from -60 to $+60$ mT) with an averaging time of 2 s. For the strongest magnetic palaeosol (S3), we performed a high resolution FORC. The field increment was 654 μT corresponding to 120 FORCs with B_u between -10 and $+10$ mT and B_c between 0 and 50 mT. Averaging time was set to 1 s. Drift corrections were performed for all measurements using the method proposed by Egli (2013). Because our samples contain SP particles, we subtracted the lower branch of the hysteresis loop from the FORC curves before processing (Egli 2013). FORC data were processed using the FORCinel package (Harrison & Feinberg 2008). We used the locally weighted regression method of Harrison and Feinberg (2008) to process the low resolution data, while for high resolution measurement we used the VARIFROC algorithm of Egli (2013).

We have selected 45 samples from the Costinești section (around 30 cm sampling interval) and 76 samples from the Mircea Vodă section (around 30 cm sampling interval) for high field isothermal remanent magnetization measurements. The sediment was filled into gel caps (about 0.6 g) and subsequently compressed and fixed with cotton wool to prevent movement of sediment particles during the measurements. Each sample was successively magnetized in three magnetic fields (1 T, 4 T and 8 T) using a MMPM 10 Pulse Magnetizer (Magnetic Measurements). After each field the samples were subjected to AF demagnetization with a peak value of 100 mT, in tumbling specimen mode, using a LDA 3A AF demagnetizer (AGICO). The remanence was measured with a JR5 spinner magnetometer. The AF demagnetization at 100 mT will remove more than 99 per cent of the signal carried by soft magnetic minerals (Maher *et al.* 2004). The remaining magnetization after 100 mT AF demagnetization (HIRM) can be considered as representing the antiferromagnetic minerals signal of hematite and/or goethite; (Maher *et al.* 2004; Deng *et al.* 2006; Zhao *et al.* 2013).

Representative samples of loess and palaeosols were subjected to detailed IRM acquisition measurements. Each sample was magnetized in 14 steps applying fields ranging from 0.1 to 8 T. After each acquisition step, the remanence was measured both before and after the AF demagnetization at 100 mT.

In addition to magnetic measurements, we also performed grain size analysis of all Costinești samples to have supplementary proxies for pedogenic process and aeolian transport. Before measurements, the samples were treated with H_2O_2 for removal of organic matter, HCl at pH 4 for removal of carbonates and dispersed with hexametaphosphate. The grain size distributions of the treated samples were measured with a Horiba laser instrument model LA950 at the Sedimentology Laboratory of the University of Bucharest.

4 RESULTS

4.1 Bulk Magnetic properties

All concentration-dependent rock magnetic parameters (χ_{lf} , χ_{ARM} and $\text{IRM}_{2\text{T}}$) show a strong contrast between loess and palaeosol horizons (Fig. 2). High values of these parameters occur in palaeosol horizons, whereas loess units are characterized by lower values. Both the loess and palaeosol horizons have a S ratio greater than 0.9 indicating that the magnetic behaviour is dominated by low coercivity magnetic minerals like magnetite and/or maghemite

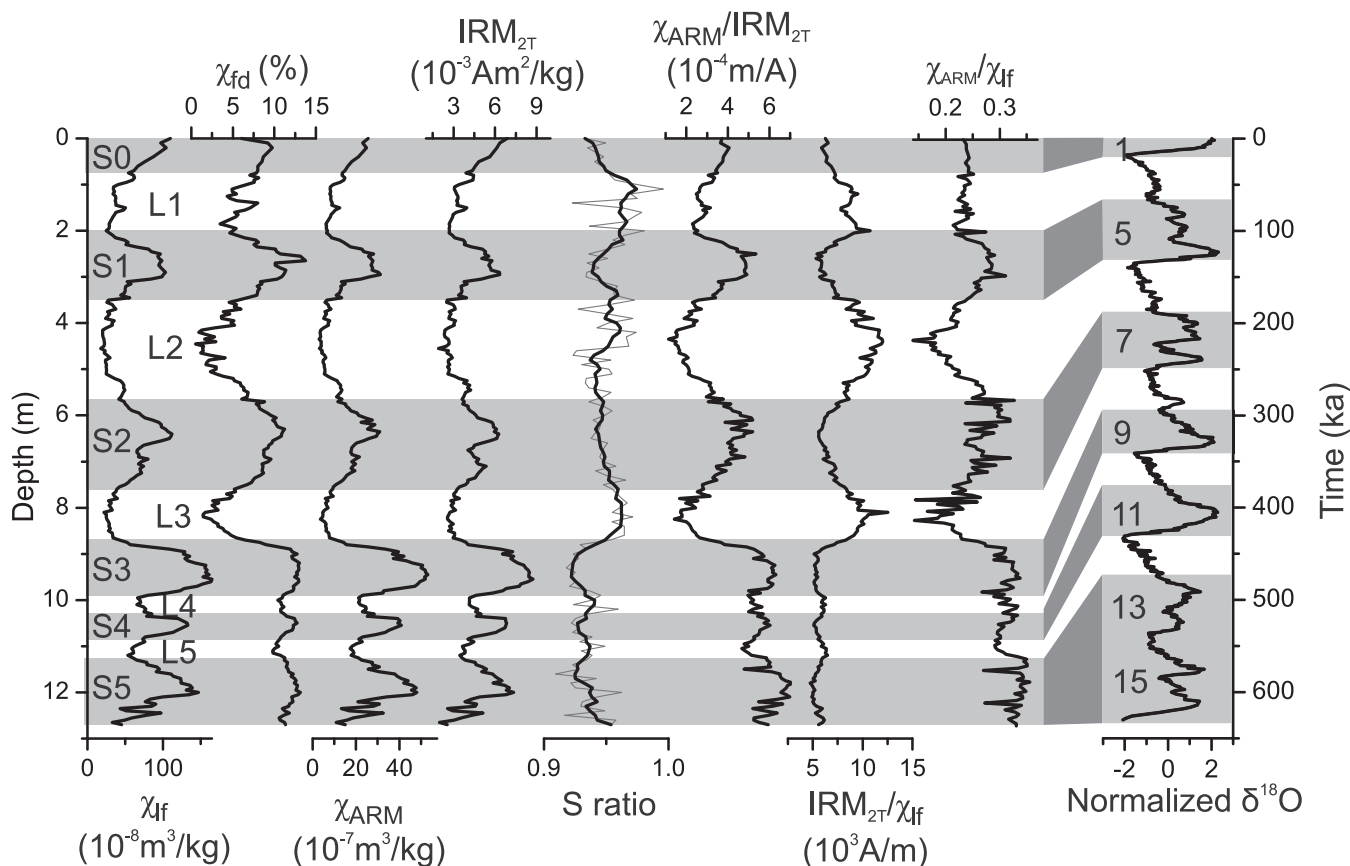


Figure 2. Magnetic properties of the Costinești loess-palaeosol deposit as a function of depth. Loess and palaeosol layers are labeled with L and S, respectively. S ratio (thin grey line) was smoothed using five points adjacent averaging (thick black line). Grey shadings mark palaeosol layers, which can be correlated to the MIS observed in a stack of 57 globally distributed $\delta^{18}\text{O}$ records (Lisiecki & Raymo 2005). The stack of 57 globally distributed $\delta^{18}\text{O}$ records was normalized to have zero mean and standard deviation of 1. The numbers to the right indicate odd MIS.

(e.g. Thompson & Oldfield 1986; Bloemendal *et al.* 1992; Liu *et al.* 2007a; Heslop 2009). The S ratio shows almost an opposite behaviour than that of the magnetic susceptibility being generally high in loess and lower in palaeosol. This suggests that palaeosols contains a higher amount of aniferromagnetic minerals than loess layers. Since χ_{ARM} preferentially responds to single domain (SD) and small pseudo-single domain (PSD) magnetite ($\sim 0.02\text{--}0.06\ \mu\text{m}$) (Maher 1988; Maher & Taylor 1988; Evans & Heller 2003), the variation of χ_{ARM} suggest that these magnetic grains size fractions are dominant in palaeosols.

The interparametric ratios like $\chi_{\text{ARM}}/\chi_{\text{LF}}$, $\chi_{\text{ARM}}/\text{IRM}_{2\text{T}}$, $\text{IRM}_{2\text{T}}/\chi_{\text{LF}}$ together with the frequency dependent magnetic susceptibility ($\chi_{\text{fd}}\%$) provide further insights into the magnetic granulometry (Fig. 2). High values of $\chi_{\text{fd}}\%$ (between 8 per cent and 13 per cent) in palaeosols show the presence of superparamagnetic particles in these horizons (Evans & Heller 1994; Forster *et al.* 1994; Dearing *et al.* 1996, 1997; Eyre 1997). In contrast, loess layers have $\chi_{\text{fd}}\%$ values less than 6 per cent. Two interparametric ratios, $\chi_{\text{ARM}}/\chi_{\text{LF}}$ and $\chi_{\text{ARM}}/\text{IRM}_{2\text{T}}$, show high values in palaeosols indicating finer magnetic grain sizes, probably SD and SP, in these horizons (Maher & Thompson 1999; Liu *et al.* 2004a; Deng 2008). Large values of $\text{IRM}_{2\text{T}}/\chi_{\text{LF}}$ and low values of $\chi_{\text{ARM}}/\chi_{\text{LF}}$ and $\chi_{\text{ARM}}/\text{IRM}_{2\text{T}}$ in loess layers suggest the presence of SD and multidomain (MD) particles in these layers (Deng *et al.* 2005; Liu *et al.* 2007b; Deng 2008).

4.2 Hysteresis properties

The Day plot ($M_{\text{rs}}/M_{\text{s}}$ versus $B_{\text{cr}}/B_{\text{c}}$) is widely used to infer the domain state of magnetic minerals (Day *et al.* 1977; Dunlop 2002a,b; Dunlop & Carter-Stiglitz 2006). Both loess and palaeosol samples are positioned in the PSD region and above the SD+MD mixing curve, similar to the Mircea Voda loess-palaeosol deposit (Necula *et al.* 2013; Fig. 3). The same position on the Day diagram was also found for loess and palaeosol data presented by several studies from Chinese loess sequences (Dunlop 2002b; Deng *et al.* 2004, 2005, 2006; Jin & Liu 2011; Chen *et al.* 2014; Song *et al.* 2014). The loess samples from L1, L2 and L3 layers are tightly grouped and closer to the SD-MD mixing curve whereas palaeosols samples are more scattered and slightly offset towards the SD-SP mixing curve. The samples from the loess layers affected by pedogenesis (L4 and L5) have a position closer to palaeosols.

FORC distributions for representative Costinești samples are similar to those found in Mircea Voda (Necula *et al.* 2013) and those from the Chaona section, a typical Chinese loess-palaeosol section (Nie *et al.* 2014; Fig. 4). Both the S2 and S3 palaeosols show small, '>' shaped open contours located just near the origin of the FORC diagram indicating the presence of SP particles (Roberts *et al.* 2000; Pike *et al.* 2001a; Roberts *et al.* 2014). They also present a narrow well defined central ridge concentrated along the B_{c} axis (at $B_{\text{u}} = 0\ \text{mT}$) representing the contribution of non-interacting SD

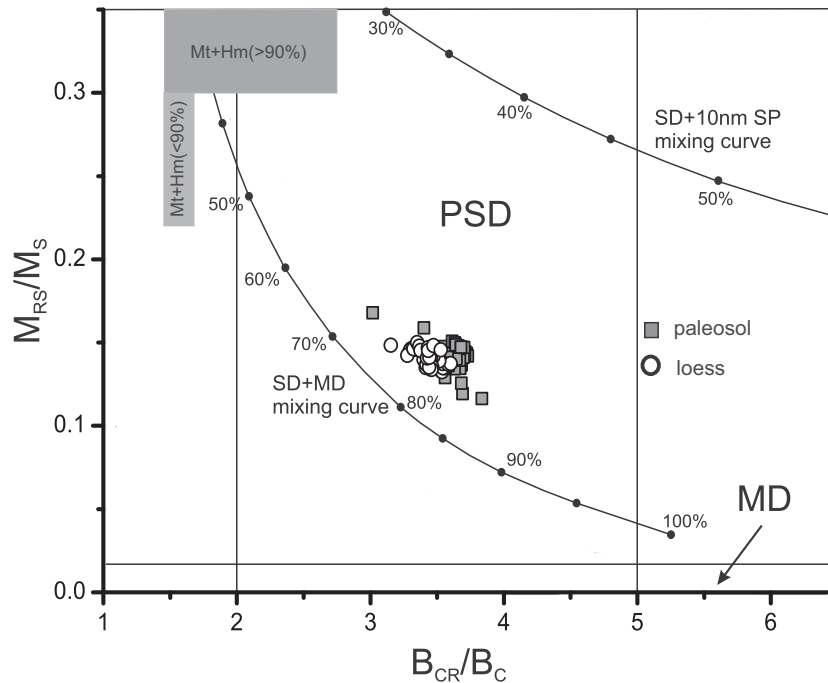


Figure 3. Hysteresis ratios of loess and palaeosol samples plotted on a Day diagram. Open circles: loess samples; grey squares: palaeosol samples. The theoretical mixing curves of Dunlop (2002a) are also plotted (the values next to the curves give the percentage of the mixture which is not SD). Grey areas mark the domain of magnetite (Mt) and hematite (Hm) mixtures (Frank & Nowaczyk 2008): dark grey = hematite content more than 90 per cent; light grey = hematite content between 0 and 90 per cent.

particles (Roberts *et al.* 2000, 2014; Geiss *et al.* 2008; Egli *et al.* 2010). All these features are clearly depicted in the high resolution FORC diagram for the S3 palaeosol. Both palaeosols show a PSD background highlighted by the small divergence and the triangular shape of outer contours (Roberts *et al.* 2000, 2014; Pike *et al.* 2001b; Nie *et al.* 2014). The S2 palaeosol shows more pronounced divergent contours that intersect the B_u axis at higher values suggesting a small increase in the contribution of the MD and/or PSD grains as compared to S3 palaeosol. L1 and L2 loess samples show more divergent behaviour of the outermost contours at low coercivities suggesting that the contribution of MD and/or PSD grains is proportionally more important than in the palaeosols (van Oorschot *et al.* 2002; Nie *et al.* 2014; Hu *et al.* 2015). The loess samples (L1 and L2) have open contours close to the ordinate axis indicating some contribution from ultrafine SP particles and a second maximum (indicated by closed contours) along the B_c -axis characteristic for noninteracting SD ferrimagnetic particles (van Oorschot *et al.* 2002; Necula *et al.* 2013; Nie *et al.* 2014). The FORC distributions show that both the loess and palaeosols contain a mixture of SP, SD and MD particles, but with a dominance of MD + SD grains in loess layers and more abundant SP+SD grains in the palaeosol horizons. These findings also explain the position of palaeosols with respect to loess in the Day's diagram (Fig. 3). Thus, the slight upward shift in the palaeosols is probably due to an increased presence of SP particles, pulling them towards the upper mixing line (Necula *et al.* 2013; Chen *et al.* 2014). The S ratio suggests that palaeosols are enriched in antiferromagnetic minerals (Fig. 2). Even the antiferromagnetic fraction contribution cannot be totally excluded, compared with the Day plot of artificial samples mixed from haematite and magnetite (Frank & Nowaczyk 2008), its manifestation in the behaviour of the palaeosol samples in the Day plot is not noticeable (Fig. 3).

4.3 Unmixing model for IRM curves

A two EMs mixing model provides a good approximation of the loess-palaeosol remanence data (Fig. 5), while addition of a third EM provides only a minor improvement in terms of the model fit. The R^2 coefficient of determination for two EMs model is 0.99924, whereas for the three end members model is 0.99936. The remanence gradient curves of the two EMs display maxima at ~ 21 and ~ 50 mT, respectively (Fig. 5). Because our loess and palaeosol samples have S ratio > 0.9 , these two EMs reflect mainly the contribution of soft ferromagnetic minerals.

The depth variation of the two EMs for the Costinesti section is plotted in Fig. 6. In the same figure we also plotted the two granulometric fractions measured at Costinesti, which are characteristic for pedogenic processes and aeolian sediment transport. Throughout the entire section, the airborne dust (particles $> 16 \mu\text{m}$) has the highest values recorded during glacial periods when wind intensity was stronger and was favourable for the transport of coarser grains (Vandenberghe *et al.* 1998; Vandenberghe & Nugteren 2001; Sun *et al.* 2002; Novothny *et al.* 2011). Both the results from the Costinesti and the Mircea Vodă (Timar-Gabor *et al.* 2011; Buggle *et al.* 2013) suggest that there is an overall trend of increasing grain size from old to young loess. The pedogenic process, which involves hydrolysis of silicate minerals leading to formation of new clay-sized minerals (particles $< 5 \mu\text{m}$ according to Buggle *et al.* 2013), are dominant in the palaeosols (above 20 per cent).

The 21 mT component (EM 1) abundance covaries with magnetic susceptibility and the pedogenic fraction, having an important contribution in all palaeosols and a minor contribution in the loess layers (Fig. 6). The 50 mT component (EM 2) variations (Fig. 6) show an inverse relationship with the 21 mT component abundance and the mass-specific magnetic susceptibility. This EM EM2 dominates the loess layers with minor contributions in palaeosols.

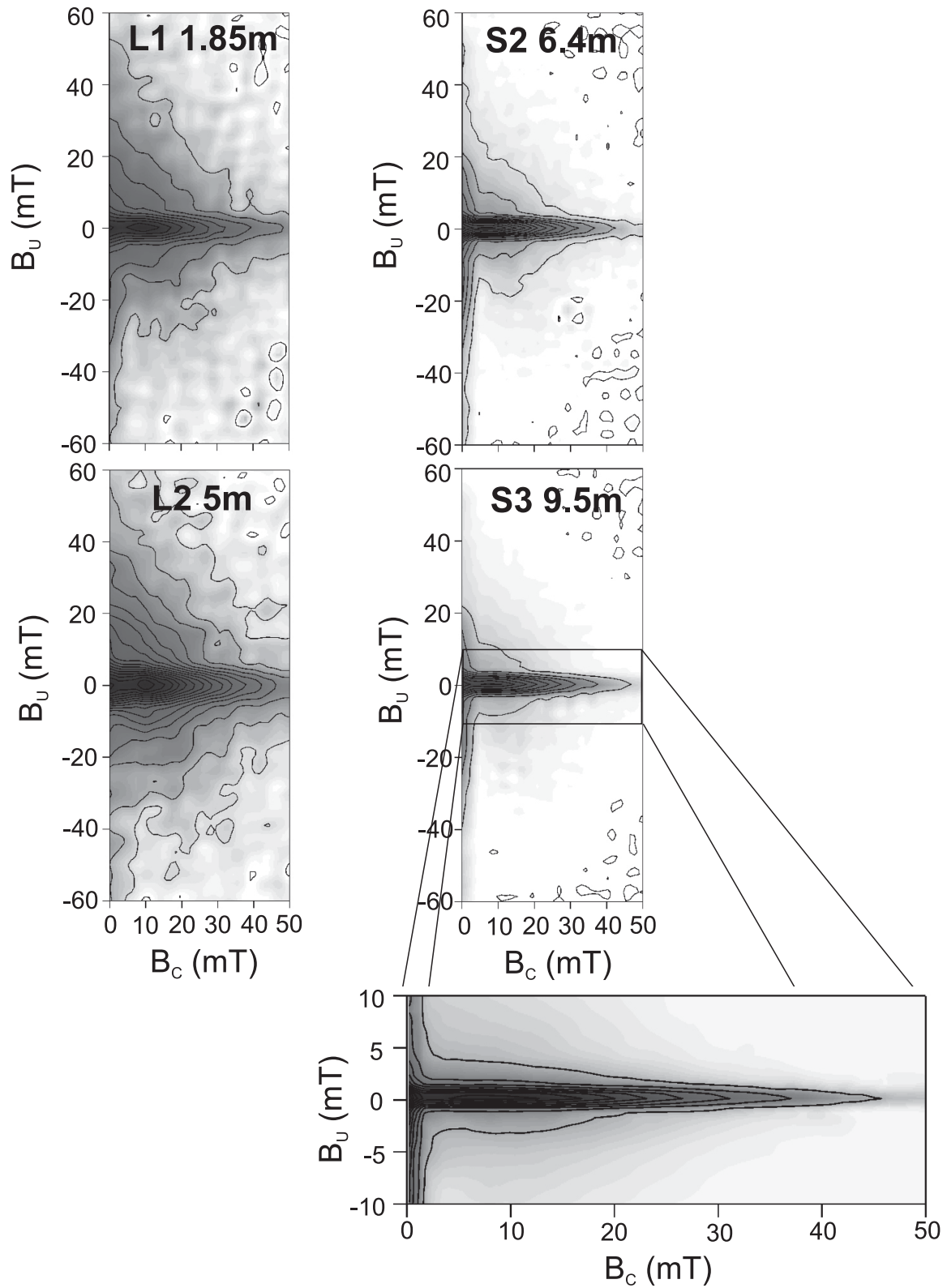


Figure 4. FORC distributions of representative samples from the Costinesti loess-palaeosol complex. We used SF = 3 for S2 and S3 palaeosols, SF = 4.5 for L1 loess and SF = 6 for L2 loess sample. For the S3 high resolution FORC we used the following VARIFORC parameters: $sc_0 = sb_0 = 3$, $sc_1 = sb_1 = 7$, $\lambda_1 = \lambda_2 = 0.1$.

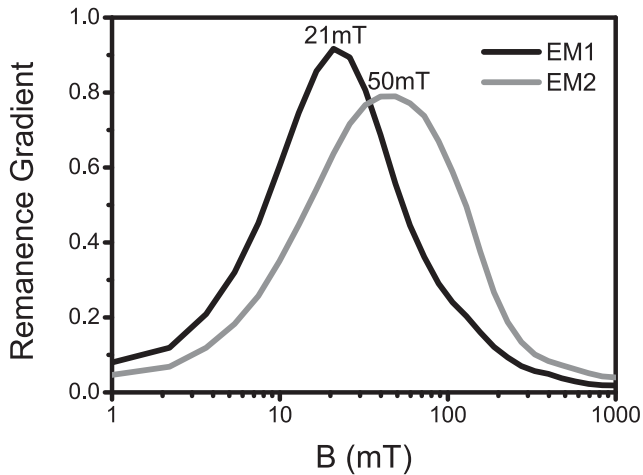


Figure 5. Remanence gradient curves calculated for the two end-member model (EM1 and EM2).

The depth variation of this component mimics the airborne dust fraction.

4.4 Hard magnetic minerals

High field IRM acquisition curves after 100 mT AF demagnetization (HIRM) for representative samples of loess and palaeosols from Mircea Voda and Costinesti deposits are displayed in Fig. 7. The HIRM acquired at 8 T is one order of magnitude lower than the IRM acquired at the same field prior the demagnetization. All HIRM acquisition curves show a rapid increase from 100 mT until 1 T in

both loess and palaeosol samples. Above 1 T the samples continue to acquire remanence up to the maximum applied field of 8 T, but with much lower rate. France & Oldfield (2000) found saturation fields between 3 and 5 T for synthetic hematite and several soils and sediments. Heller (1978) has shown that goethite displays only weak remanences in fields up to 4 T. Therefore the signal up to 4 T is mainly dominated by hematite. The increase of all HIRM acquisition curves beyond 4 T can reflect a weak contribution from goethite, which did not saturate even in fields up to 57 T (Rochette & Fillion 1989).

Figs 8 and 9 present results of the HIRM measurements for the Mircea Vodă and Costinești sections. $\text{HIRM}_{1\text{T}}$ and $\text{HIRM}_{4\text{T}}$ (HIRM acquired in field of 1 and 4 T, respectively) are likely to be mainly dominated by a hematite contribution (Heller 1978; France & Oldfield 2000; Maher *et al.* 2004; Hao *et al.* 2009). To preclude any contribution of low-coercivity minerals we subtracted the $\text{HIRM}_{1\text{T}}$ from the $\text{HIRM}_{4\text{T}}$ ($\text{HIRM}_{4-1\text{T}}$). Remanence acquisition between 4 and 8 T ($\text{HIRM}_{8-4\text{T}}$) is thought to reflect the contribution from goethite (Walden *et al.* 1999; France & Oldfield 2000; Hao *et al.* 2009; Maher *et al.* 2004).

$\text{HIRM}_{4-1\text{T}}$ measurements show low values in the loess layers and higher values in the palaeosols (Figs 8 and 9), suggesting an increase in hematite contribution during interglacial periods. $\text{HIRM}_{8-4\text{T}}$ values are more than three times weaker than the $\text{HIRM}_{4-1\text{T}}$ values, indicating that very little remanence is acquired above 4 T. The inferred goethite contribution represented by $\text{HIRM}_{8-4\text{T}}$ measurements shows no clear contrast between loess and palaeosols horizons both for the Mircea Vodă section and the Costinesti section. Only in the lower part of the Mircea Vodă section, in palaeosol S5, the $\text{HIRM}_{8-4\text{T}}$ variations are similar to the $\text{HIRM}_{4-1\text{T}}$ variations.

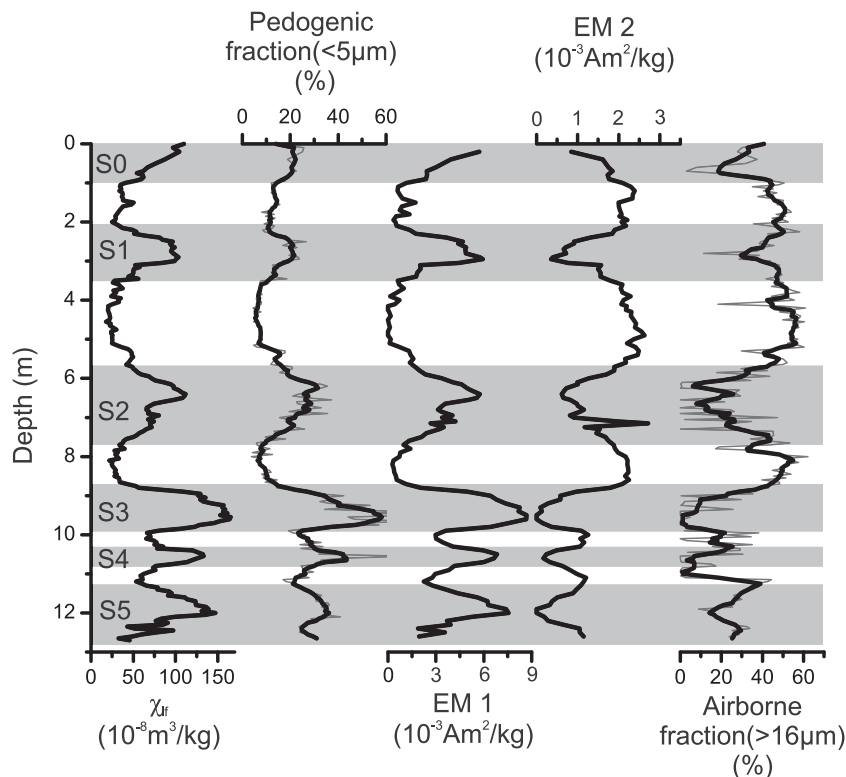


Figure 6. Remanence contributions of the two individual end-members (EM1 and EM2), magnetic susceptibility, grain size distribution of the clay (<5 μm) and airborne fractions (>16 μm) versus depth. The grain size distributions were smoothed using 5 points adjacent averaging. Grey shadings mark the palaeosol units.

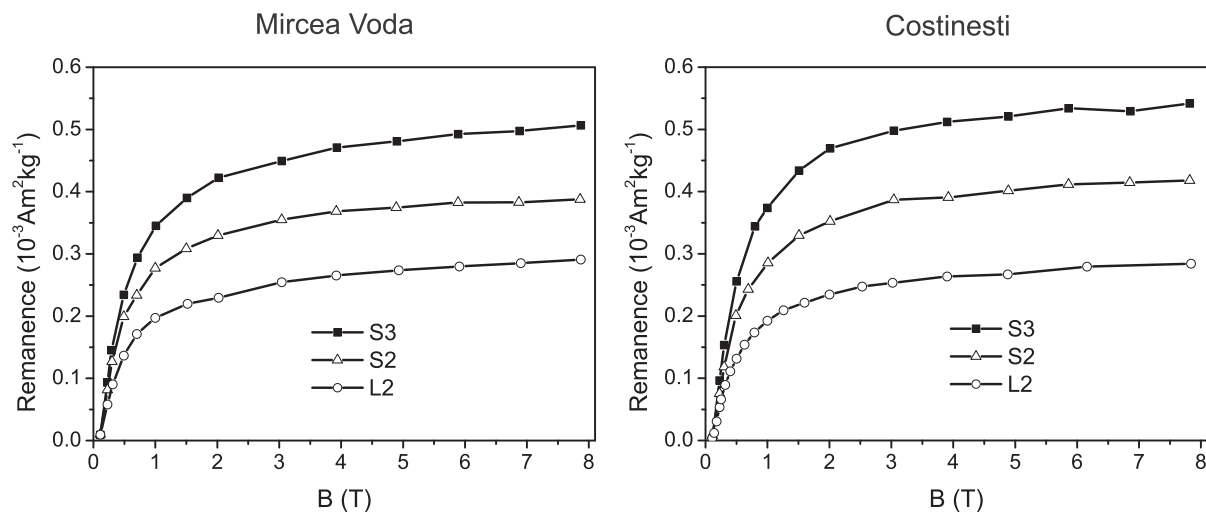


Figure 7. HIRM acquired in fields up to 8 T after 100 m AF demagnetization for representative samples from S3 (forest soils) and S2 (chernozems) palaeosols and L2 loess unit of the Mircea Voda and Costinești sections.

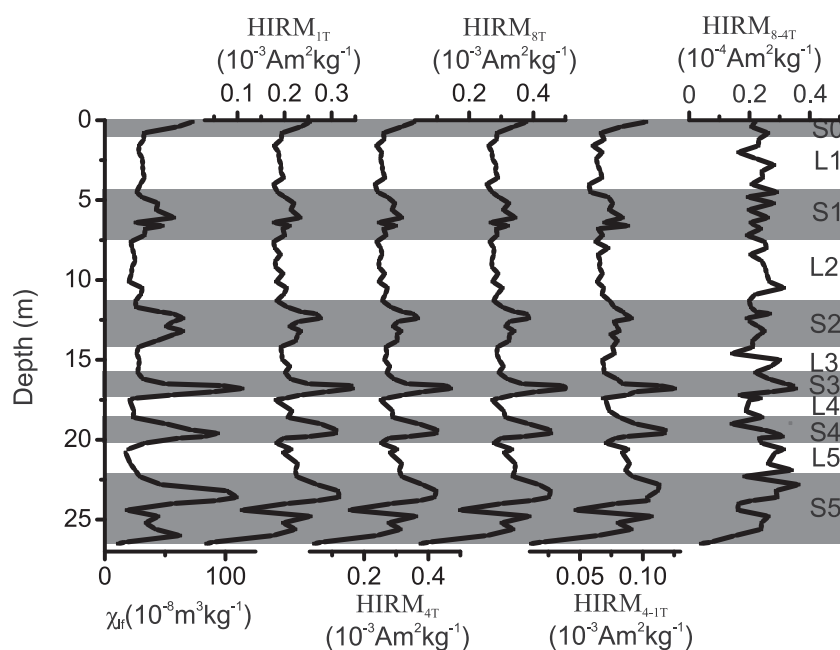


Figure 8. Mircea Vodă loess-palaeosol section: low field magnetic susceptibility (χ_{lf}) and HIRM acquired in fields of 1, 4 and 8 T after 100 mT AF. $HIRM_{4-1T} = HIRM_{4T} - HIRM_{1T}$ represents hematite contribution free from any ferrimagnetic influence. $HIRM_{8-4T} = HIRM_{8T} - HIRM_{4T}$ reflects mainly goethite contribution.

5 DISCUSSIONS

5.1 Origin of ferromagnetic minerals

5.1.1 Soft ferromagnetic minerals

The variations of several rock magnetic parameters (χ_{lf} , χ_{ARM} , $\chi_{fd}\%$, χ_{ARM}/χ_{LF} , χ_{ARM}/IRM_{2T} , IRM_{2T}/χ_{LF} , hysteresis properties) are mainly controlled by the contribution of soft coercivity magnetic minerals (magnetite and maghemite). All these data show that magnetic enhancement in the recent soil and palaeosols is mainly produced by a mixture of fine magnetic grains (SP, SD and PSD) in contrast to the loess layers (L1, L2 and L3) where SD and MD magnetic grains are dominant. At Costinești, the thin loess layers L4 and L5 have a significant contribution from fine magnetic grains with respect to the thicker upper loess layers.

The unmixing model for IRM curves (Fig. 6) shows the presence of two components: a 21 mT component (EM 1) and a 50 mT component (EM 2). The component EM1 is probably of pedogenic origin because it covaries with the pedogenic granulometric fraction and have an important contribution in all palaeosols and a minor contribution in the loess layers. Using the same method, the 21 mT pedogenic component was also found dominant in the palaeosol layers from the Mircea Voda section (Necula *et al.* 2013) and the Chaona loess section (Chinese Loess Plateau, Nie *et al.* 2014). Other IRM decompositions, obtained using different methods, showed peaks coercivities for pedogenic magnetite/maghemite of ~ 21 mT (Lingtai section, Chinese Loess Plateau, Spassov *et al.* 2003) and ~ 25 mT (Luochuan section, Chinese Loess Plateau, Hu *et al.* 2013). Jordanova *et al.* (2011) also found a similar pedogenic phase with a very stable mean coercivity of ~ 31 mT in all palaeosol

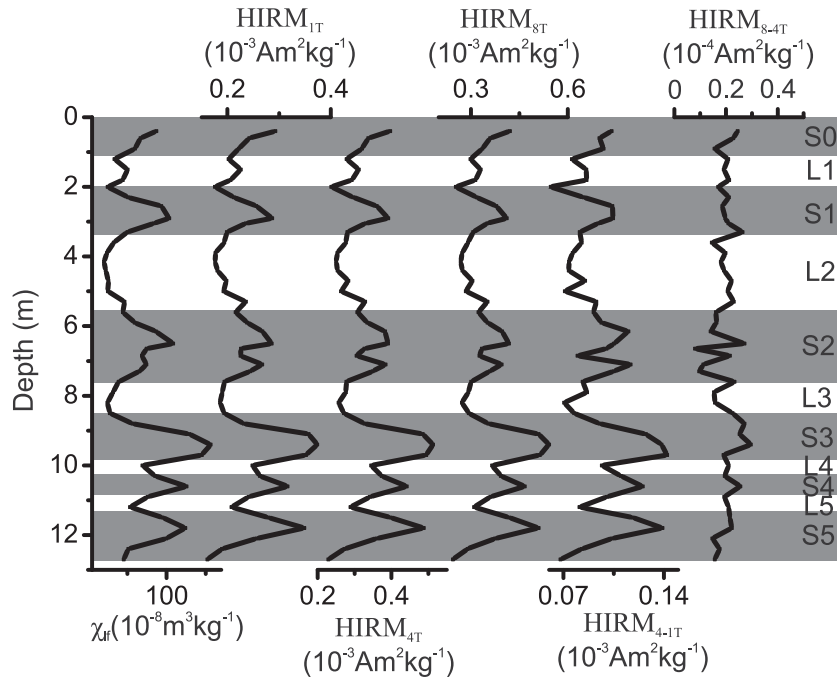


Figure 9. Costinești loess-palaeosol section: low field magnetic susceptibility (χ_{ir}) and HIRM acquired in fields of 1, 4 and 8 T after 100 mT AF. $HIRM_{4-1T} = HIRM_{4T} - HIRM_{1T}$ represents hematite contribution free from any ferrimagnetic influence. $HIRM_{8-4T} = HIRM_{8T} - HIRM_{4T}$ reflects mainly goethite contribution.

samples collected from four Bulgarian loess-palaeosol deposits (Orsoja, Koriten, Lubenovo and Durankulak). Following these studies we interpret the 21 mT component from the Costinești section as representing pedogenic magnetite grains around the SP/SSD boundary, but which are large enough to carry stable remanences for the duration of the experiments.

The component EM2 variations are similar to the airborne dust fraction (Fig. 6) and dominate the loess layers with minor contributions in palaeosols. Necula *et al.* (2013) found a hard detrital component (~ 60 mT) in the nearby Mircea Voda section. Nie *et al.* (2014) identified in the Chaona loess section a similar hard detrital component peaking at 72 mT. Using Gaussian functions to decompose the IRM signal, Jordanova *et al.* (2011) found a fairly uniform detrital component with coercivity peaking at ~ 58 mT in loess samples from the Koriten and the Lubenovo loess-palaeosol sections. In the Chinese Loess Plateau, Spassov *et al.* (2003) found a 79 mT component in the Lingtai loess samples and Hu *et al.* (2013) identified a dominant component in the Luochuan loess samples peaking at the same coercivity as our component. All these studies have interpreted this component as being carried by a detrital magnetite or partially oxidized detrital magnetite (magnetite core with maghemite rim resulting from weathering). Theoretically, for PSD magnetite, coercivity should decrease dramatically with increasing grain size (Dunlop & Özdemir 1997; Maher 1988). However, according to van Velzen and Dekkers (1999) the stress induced by surface oxidation increases the coercivity of the particle, therefore oxidized aeolian PSD/MD grained magnetite becomes harder. Based on measurements on synthetic samples and micromagnetic modelling, Ge *et al.* (2014) showed that for large PSD grains (> 110 nm) the coercivity increase, with a sudden decrease when the maghemitization is complete. In addition, they found that for small PSD particles (80–100 nm, close to the SD/PSD boundary) there is a gradual magnetic hardening until the core disappears due to a reduction of magnetization as the maghemite skin grows. Our FORC

distributions for the loess samples showed a significant contribution from PSD/MD magnetite in these horizons (Fig. 4), which is also reflected in the high values of χ_{ARM}/χ_{LF} in loess layers (Fig. 2). In consequence the second component provided by unmixing the IRM acquisition curves most probably reflect a contribution from oxidized PSD/MD detrital magnetite of aeolian origin.

All these results show that magnetic enhancement at Costinești can be explained by the pedogenic model, that is, the *in situ* production of new soft ferrimagnetic minerals during soil formation (Maher & Thompson 1991; Evans & Heller 1994; Hunt *et al.* 1995). The magnetic properties of the first three loess layers are dominated by soft ferrimagnetic minerals of aeolian origin. The lower thin loess layers (L4 and L5) present significant enhancement in comparison with the younger loess units above, suggesting that these loess layers are intensely affected by pedogenesis.

5.1.2 Hematite

The $HIRM_{4-1T}$ parameter presents low values in loess units and higher values in palaeosols. This illustrates a significant increase in hematite contribution during interglacial periods, suggesting a pedogenic origin. The result is in agreement with Buggle *et al.* (2014), who also found high concentrations of hematite of pedogenic origin in the Mircea Voda palaeosols using DRS in combination with rock magnetic measurements. Jordanova *et al.* (2011), using both DRS and rock magnetic methods, has concluded that the pedogenesis is accompanied by preferential formation of hematite over goethite in all analysed sites from Bulgaria. Similar hematite enrichment in the Late Pleistocene soils was found in the Middle Danube Basin (Batajnica/Stari Slankamen and Orlovat loess-palaeosol sequences) by Buggle *et al.* (2014) and Lukić *et al.* (2014) using rock magnetic and colorimetric measurements. There are many studies which also reported more abundant hematite of pedogenic origin in palaeosols from the Chinese Loess Plateau and Tibetan loess (e.g. Liu *et al.*

2004b,c; Deng *et al.* 2006; Zhang *et al.* 2009; Chen *et al.* 2010; Hu *et al.* 2013, 2015; Zhao *et al.* 2013). The occurrence of pedogenic hematite generally indicates stronger weathering intensity under a warm and humid, but seasonally dry soil forming condition (Cornell & Schwertmann 2003; Deng *et al.* 2006; Zhang *et al.* 2009, 2012; Chen *et al.* 2010). The increasing DRS derived weathering degree index in Bulgarian palaeosols indicates a higher degree of low-temperature oxidation during pedogenesis resulting in formation of pedogenic hematite (Jordanova *et al.* 2011). At the Costinești and Mircea Vodă sections the highest values of the hematite signal can be found in S3, S4 and S5 palaeosols implying that these palaeosols were formed under significantly warmer and seasonally more humid conditions than the soils formed later. This feature is also observed in the DRS measurements from the Mircea Vodă section and according to Buggle *et al.* (2014) reflects the transition from the Mediterranean climate to the steppe climate. The high correlation between the pedogenic soft magnetic minerals and hematite concentrations supports the hypothesis that these two minerals form concomitantly (Torrent *et al.* 2007).

Inside the loess layers the hematite contributions have lower values than in palaeosols. Both magnetic and granulometric data indicate the absence of important pedogenic alteration in these loess units. According to Chen *et al.* (2014), the hematite particles found in these loess portions are rather of detrital origin. Jordanova *et al.* (2011) supposed that the hematite found in the loess layers from the Durankulak section situated on the Black Sea coast came from aeolian dust blown from local dust sources during glacial periods. We also favour the hypothesis that the hematite in our loess layers is mainly of aeolian origin. At Mircea Vodă, magnetic measurements are more efficient to prove the presence of hematite during glacial periods than sole DRS measurements, which suggest the absence of hematite during loess deposition (Buggle *et al.* 2014).

5.1.3 Goethite

The inferred goethite contribution represented by $HIRM_{8-4T}$ (Figs 8 and 9) presents no systematic contrast between loess and palaeosols horizons both at the Mircea Voda section and the Costinești section. $HIRM_{8-4T}$ values indicate that the goethite contribution is almost constant. The small gain in remanence between 4 and 8 T may result in a high degree of uncertainties in the $HIRM_{8-4T}$ parameter which can mask the real goethite contribution (Hao *et al.* 2009). Moreover goethite may acquire significant remanence in fields higher than those used in this study (e.g. Dekkers *et al.* 1989), so an 8 T magnetic field intensity might not be enough to recover the true goethite contribution (Hao *et al.* 2009). Maher *et al.* (2004) have shown that synthetic hematite powders continue to acquire remanence in applied dc fields of up to 7 T, although at a much lower rate than that of goethite. This behaviour of hematite can further complicate the interpretation of $HIRM_{8-4T}$ and can explain the similarities between $HIRM_{4-1T}$ and $HIRM_{8-1T}$ in the lower part of the Mircea Vodă section (Fig. 8).

Based on DRS measurements, Torrent *et al.* (2007) and Hu *et al.* (2015) found no correlation between goethite concentration and frequency dependent magnetic susceptibility in loess sections from the Chinese Loess Plateau and Tibetan Plateau, respectively. They proposed that goethite formation is probably independent of pedogenesis. The Rubification Index of palaeosols at Mircea Vodă site (Buggle *et al.* 2014) suggests the presence of goethite in loess layers without significant variability. Because there is no clear correlation

between the $HIRM_{8-4T}$ parameter and lithology we presume, similar to Torrent *et al.* (2007), that goethite is probably of aeolian origin.

5.2 Correlation of loess-palaeosol deposits from the lower Danube basin during the Brunhes chron

To correlate the loess-palaeosol deposits from the lower Danube basin, we have used the magnetic susceptibility curves, because there is a strong correlation between magnetic susceptibility and lithology, and geochronological controls. Fig. 10 summarizes the longest magnetic susceptibility profiles from the lower Danube basin extending through the Brunhes chron. From west to east (Fig. 1) these profiles are: Lubenovo and Viatovo (Bulgaria, Jordanova *et al.* 2007, 2011), Zimnicea (Romania, Rădan 2012), Mostiștea (Romania, Panaiotu *et al.* 2001; Necula & Panaiotu 2008), Koriten (Bulgaria, Jordanova & Petersen 1999), Mircea Vodă (Romania, Buggle *et al.* 2009; Necula *et al.* 2013), Costinești (Romania, this study), Primorskoje (Ukraine, Nawrocki *et al.* 1999) and Nova Etuliya (Moldavia, Tsatskin *et al.* 2001; Gendler *et al.* 2006; Tsatskin *et al.* 2008). All these loess-palaeosol sections belong to the loess deposit area D5 defined by Smalley *et al.* (2009) in the lower Danube basin. According to Smalley *et al.* (2009) the loess in this area is essentially mountain loess, derived from the Carpathians and other high regions surrounding the lower Danube basin. Buggle *et al.* (2008) have shown that the loess from the Dobrogea is predominantly derived from the Danube alluvium.

We have used two types of geochronological controls for the loess sections presented in Fig. 10: direct dating by luminescence and palaeomagnetic dating (position of Matuyama–Brunhes boundary). Direct dating for the loess sections from the lower Danube basin is available only for three of these locations: Mostiștea (Balescu *et al.* 2010; Vasiliniuc *et al.* 2011), Mircea Vodă (Balescu *et al.* 2010; Timar *et al.* 2010; Timar-Gabor *et al.* 2011; Vasiliniuc *et al.* 2012) and Costinești (Balescu *et al.* 2003; Constantin *et al.* 2014). Several luminescence methods (IRSL on feldspar, elevated temperature post-IR IRSL signals and OSL) have shown that the first four loess layers from Mostiștea, Mircea Vodă and Costinești can be correlated with MIS 2–4, MIS 6, MIS 8 and MIS 10 and the palaeosols (S1, S2 and S3 in Fig. 10) below these layers with MIS 5, MIS 7 and MIS 9.

The position of Matuyama–Brunhes (M–B) boundary is well documented for two sections: Viatovo (Jordanova *et al.* 2008) and Nova Etuliya (Gendler *et al.* 2006). At Viatovo, the M–B boundary was found in the loess layer below the pedocomplex S6 (Fig. 10). At Nova Etuliya, the M–B boundary was found in the pedocomplex PK7 (Fig. 10). According to the palaeomagnetic data both sections extend below the M–B boundary, but our discussion will be limited to the Brunhes chron. There are two reports about the presence of M–B boundary below the pedocomplex S6 (Fig. S4) at the base of the Costinești (Tuzla) section (Balescu *et al.* 2003) and below pedocomplex S6 in the Zimnicea borehole (Rădan 2012). Both reports should be regarded as preliminary, because they are based on a limited number of samples. Nawrocki *et al.* (1999) found only normal polarity at the Primorskoje section and concluded that it was deposited during Brunhes chron. Position of the M–B boundary in the Lower Danube Basin below the pedocomplex S6 is in agreement with the results from the Middle Danube Basin (e.g. Fitzsimmons *et al.* 2012), the Transcarpathia region (Nawrocki *et al.* 2015) and the East Carpathian Foreland (Nawrocki *et al.* 2002).

Because these geochronological markers are not available for all the sections, to correlate them it is necessary to accept a supplementary hypothesis concerning the formation of palaeosols with strong

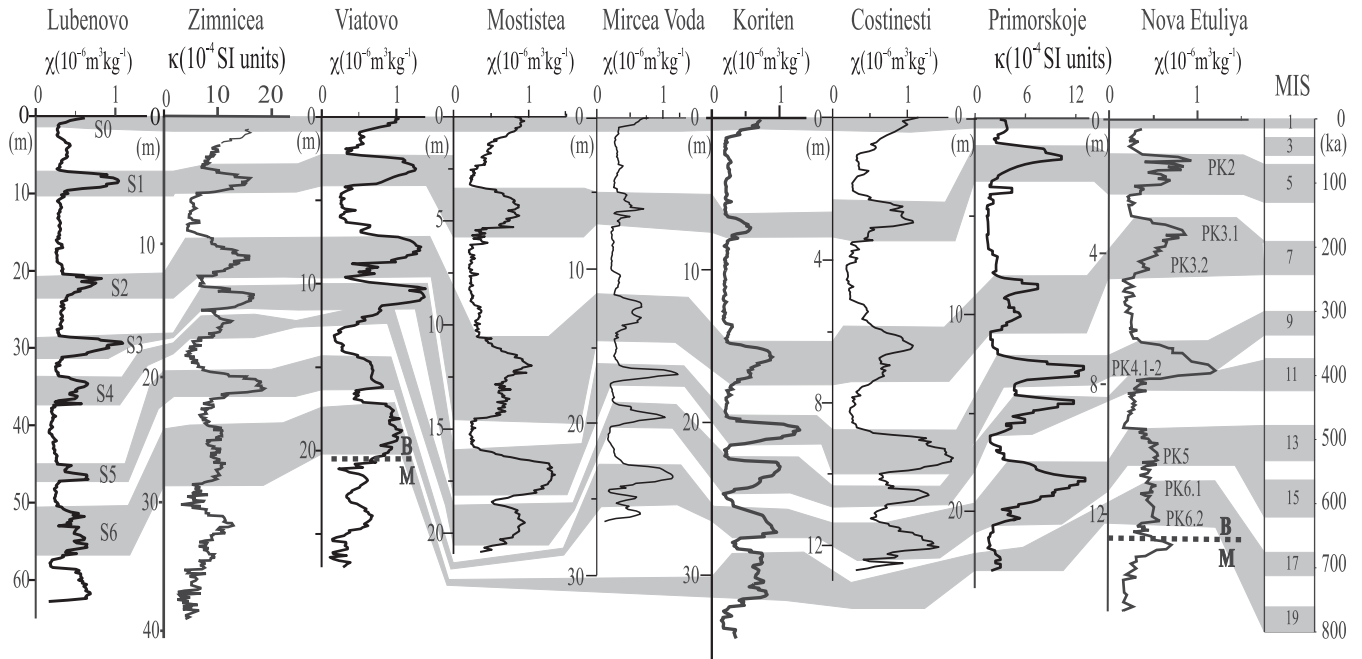


Figure 10. Correlation of the loess-palaeosol sections from the lower Danube basin. The recent soil (S0) and the palaeosols (S1–S6) and their correlation with MIS are marked by grey bands. MIS stages boundaries are after Lisiecki and Raymo (2005). Matuyama (M)–Brunhes (B) boundary is marked with a dash line. The positions of pedocomplexes (PK) from Nova Etuliya are after Tsatskin *et al.* (2008).

magnetic enhancement. Since the pioneering work of Jordanova & Petersen (1999) at Koriten, it is accepted that the palaeosols from the lower and middle Danube basin with strong magnetic enhancement are formed during odd MIS (e.g. Fitzsimmons *et al.* 2012 and references therein). However, in the absence of direct dating of each section, field observations concerning absence or presence of significant erosion or a palaeosol with a particular susceptibility pattern are necessary to correlate both the palaeosols with each other and with corresponding MIS. Important erosions are not reported for any sections presented in Fig. 10. The best regional reference palaeosol is the one labelled S2 in Fig. 10 (Panaiotu *et al.* 2001; Jordanova *et al.* 2007; Fitzsimmons *et al.* 2012). This is a double palaeosol which can be observed both in the field (e.g. Figs S5 and S6) and in the magnetic susceptibility profiles as a more or less pronounced double peak (Fig. 10). In the lower part of the overlying loess layer L2 an incipient palaeosol can be observed as a small peak in the magnetic susceptibility curves (Fig. 10). This pattern was described on several sections from lower Danube basin: Lubenovo and Viatovo (Jordanova *et al.* 2007), Mostiștea (Panaiotu *et al.* 2001), Koriten (Jordanova & Petersen 1999), Mircea Vodă (Bugge *et al.* 2009; Necula *et al.* 2013) and Costinești (this study). This succession of three palaeosols can be observed also in the loess sections from the middle Danube basin (Panaiotu *et al.* 2001; Fitzsimmons *et al.* 2012). The same pattern of oscillations of the magnetic susceptibility can be observed in the Chinese loess sections in the loess L2 (assigned to MIS 6) and palaeosol S2 (assigned to MIS 7; e.g. Heslop *et al.* 2002; Fitzsimmons *et al.* 2012; Marković *et al.* 2012).

The MIS 7 reference palaeosol is also evident in the Primorskoje section (Fig. 10). Since recent luminescence dating have shown that this double palaeosol S2 correspond to MIS 7 and the magnetic susceptibility profile from the Primorskoje section is almost identical with the one measured at Costinești, we think that the chronology proposed by Nawrocki *et al.* (1999) must be abandoned. This chronology was based on old ^{14}C and luminescence ages and proposed the correlation of palaeosol S2 with MIS 3 and the following

palaeosols (labelled S3, S4 and S5 in Fig. 10) with MIS 5, MIS 7 and MIS 9–13.

Having the palaeosol S2 as reference and the hypothesis that each palaeosol with a strong magnetic susceptibility corresponds to about an odd MIS, both the correlation of the sections each other and with marine isotope stages is robust for the first five palaeosols (Jordanova & Petersen 1999; Panaiotu *et al.* 2001; Jordanova *et al.* 2007; Bugge *et al.* 2009; Rădan 2012; Necula *et al.* 2013). For the Primorskoje section, based on magnetic susceptibility curve, we proposed the same correlation of palaeosols as for the rest of sections: S1 corresponds to MIS 5, S2 corresponds to MIS 7, S3 corresponds to MIS 9, S4 corresponds to MIS 11 and S5 corresponds to MIS 13–15. At Viatovo (Jordanova *et al.* 2007, 2008) there is a pedocomplex above M–B boundary (labelled S6 in Fig. 10) which is separated by a loess layer from the palaeosol S5. The same pattern can be observed also at the other long sections Lubenovo (Jordanova *et al.* 2007), Zimnicea (Rădan 2012) and Koriten (Jordanova and Petersen 1999). Due to the lack of clear expression of loess layers both in the field and in the magnetic susceptibility curve, this pedocomplex is correlated with the time interval from MIS 17–MIS 19 (Jordanova & Petersen 1999; Jordanova *et al.* 2007; Fitzsimmons *et al.* 2012; Rădan 2012).

The correlation of the Nova Etuliya section with the rest of the lower Danube basin sections is not straightforward. Tsatskin *et al.* (2001) proposed the following scheme of correlation of the seven palaeosols observed above B–M boundary at the Nova Etuliya with MIS: the first pedocomplex PK1 is correlated with MIS 5, the second pedocomplex PK2 is correlated with MIS 7, MIS 9 and MIS 11, the third pedocomplex PK4 is correlated with MIS 13–15, the fourth pedocomplex PK5 with MIS 17 and the pedocomplex PK6 is correlated with MIS 19. This scheme is not supported by any direct dating. The pedocomplex PK4, characterized by the highest magnetic susceptibility peak, is considered a stratigraphic marker for the loess-palaeosol sections from Moldavia and south Ukraine (Tsatskin *et al.* 2001; Dodonov *et al.* 2006) and it is traditionally

associated with MIS 13–15 (Tsatskin *et al.* 1998, 2001, 2008). In the rest of the loess-palaeosol sections from Dobrogea (Koriten, Mircea Vodă, Costinești, Fig. 10) the highest magnetic susceptibility is reached in the brown–red palaeosol S3, which is correlated with MIS 9. Since large climatic differences of Nova Etuliya with respect to the Dobrogea sections are unlikely due to the close distance, therefore we propose the following scheme to correlate this section with the other sequences in the area (Fig. 10). The first pedocomplex PK1 corresponds to palaeosol S1 from the other sections and to MIS 5 in agreement with Tsatskin *et al.* (2001). The second pedocomplex PK2 formed by two welded palaeosols (Tsatskin *et al.* 2008) corresponds to the double palaeosol S2 clearly observed in other sections and to MIS 7. Below S2 all the sections from the Dobrogea plateau present three well define susceptibility peaks correlated with MIS 9, 11 and 13–15. At Nova Etuliya there is only one peak corresponding to the pedocomplex PK4. This pedocomplex, which has the highest magnetic susceptibility, is formed by two welded palaeosols (Tsatskin *et al.* 2008). Because the loess layer deposited between palaeosol S3 and S4 is thin and sometimes affected by pedogenesis in most of the loess sections from the lower Danube basin (Fig. 10), we propose to correlate the pedocomplex PK4 with S3 and S4 corresponding to MIS 9 and MIS 11. A similar stack of the palaeosols S3 and S4 was reported for the Viatovo section (Jordanova *et al.* 2007) and Zimnicea section (Rădan 2012). Below PK4, there are three palaeosols, which are characterized by relative low magnetic susceptibility values. Tsatskin *et al.* (2008) presume that semihydromorphic and hence reducing conditions in the soils are the possible explanation for the posterior destruction of magnetite in PK5 and PK6. Taking the position of M-B boundary at Nova Etulya into account, we tentatively correlate PK5 with S5 and MIS 13–15 and PK6 with S6 and MIS 17–19. If our correlation scheme will be confirmed by direct luminescence dating of the upper loess layers, it will also impose the re-evaluation of the age of pedocomplex PK4 (Virina palaeosol) from the Roxolani loess section (Tsatskin *et al.* 1998) and from the other loess sections from the East European low lands where it is considered an important stratigraphic marker (Dodonov *et al.* 2006).

The magnetic susceptibility data from the eastern part of the lower Danube basin (Mircea Vodă, Koriten, Costinești and Primorskoje) can be interpreted as support for the transition of a Mediterranean type climate to a steppe type climate (Bugge *et al.* 2014). This transition is reflected in the higher magnetic susceptibility values of the palaeosols S5, S4 and S3, formed between 630 and 330 ka, with respect to later palaeosols. This pattern is less visible at Mostiștea and Zimnicea and completely reversed at Viatovo and Lubenovo where the highest magnetic susceptibility values are recorded in palaeosols S1, S2 and S3 (Jordanova *et al.* 2007). Marković *et al.* (2011), Fitzsimmons *et al.* (2012) and Bugge *et al.* (2014) suggest that the rock magnetic data from the Middle and Lower Danube basins are in agreement with a precipitation gradient from east to west across the basin during the Pleistocene. On the other hand Jordanova *et al.* (2007) proposed that local factors, as elevation of the loess sections, probably control this pattern of magnetic susceptibility values. We propose that this contrasting pattern of magnetic susceptibility data over a relative short distance (~300 km) reflect the local climatic influence of the Black Sea overlap with continental scale climatic oscillations in Southern Europe during the Brunhes chron. However the quantitative interpretation of magnetic susceptibility data from the Danube basin palaeosols to estimate the precipitation rate (Panaiotu *et al.* 2001; Bugge *et al.* 2009, 2013) must be made with caution, because magnetic climatic functions can be affected by large errors (Heslop & Roberts 2013) and

complex factors (the frequency of drying/wetting cycles and the average moisture of the soil) control the magnetic enhancement factors of loessic soils (Orgeira *et al.* 2011). An alternative explanation for the transition of a Mediterranean type climate to a steppe type climate was proposed by Bugge *et al.* (2013, 2014). They proposed that the progressive aridification in SE Europe is mainly caused by the elevation increase of surrounding mountain belts. In our opinion this explanation needs more arguments both because these changes in palaeoelevation were probable small and their amplitude is not well constrained (Bugge *et al.* 2013) and because the amplitude of climatic influence of these small changes in the elevation of the Alps and Carpathians Mountains is not yet evaluated by any climatic model.

Background magnetic susceptibility values of the Romanian loess-palaeosol sections are presented in Table 1. According to Forster *et al.* (1994) background magnetic susceptibility values characterize the magnetic susceptibility of the dust from the source area. To look for a possible change in the source area of the dust, we have computed these background magnetic susceptibilities both for the steppe type climate (samples from S0 to L3) and the Mediterranean type climate (samples from S3 to the end of the section). The background magnetic susceptibility values for the Mediterranean type climate are significant lower than similar values for the steppe type climate for all sections. This result indicates contributions from two different source areas of dust during the climatic transition. According to Bugge *et al.* (2008), the loess of the Dobrogea plateau (Romania) is predominantly derived from Danube alluvium with a minor source derived from the Ukrainian glaciofluvial deposits. Bugge *et al.* (2008) also found distinctly lower values of magnetic background susceptibility in the sites from Ukraine with respect to the sites from the Lower Danube Basin. Taking into account their results, we proposed that the dust transport from the Ukrainian glaciofluvial deposits, which are characterized by lower values of background magnetic susceptibility ($\sim 8 \times 10^{-8} \text{ m}^3 \text{ kg}^{-1}$), was probably enhanced during the Mediterranean type climate. The transition to a steppe type climate is accompanied by a change to a dominant source area derived from Danube alluvium, which are characterized by larger values of background magnetic susceptibility ($\sim 20 \times 10^{-8} \text{ m}^3 \text{ kg}^{-1}$). The Mostiștea and Mircea Vodă sections has always larger values of background magnetic susceptibility than the Costinești section, because they are closer to the source area derived from Danube alluvium.

6 CONCLUSIONS

Detailed bulk rock magnetic measurements of the Costinești loess/palaeosol section from the Black Sea shore have resulted in the following conclusions about magnetic mineralogy and its climatic control:

- (1) The magnetic enhancement of palaeosol horizons in the Costinești sequence is produced mainly by pedogenic soft magnetic minerals, which include ultrafine grained SP, grains at the SP/SD threshold, stable SD grains and PSD magnetite/maghemite grains. Small amounts of coarser magnetic grains of aeolian origin can also be present in the palaeosols.
- (2) The loess layers in Costinești are dominated by MD and/or PSD oxidized magnetite of aeolian origin. Some contribution from SD and SP/SD grains is also present, suggesting an incipient degree of pedogenesis during loess accumulation.
- (3) The unmixing model for IRM curves shows the presence of two components with different coercivity. The first coercivity

Table 1. Background magnetic susceptibility values (χ_{bg}) of the Romanian loess-palaeosol sections and their 95 confidence limits.

Loess-palaeosols	Climate	Costinești χ_{bg} ($m^3 kg^{-1}$)	Mircea Vodă χ_{bg} ($m^3 kg^{-1}$)	Mostiștea χ_{bg} ($m^3 kg^{-1}$)
S0–L3	Steppe	17.11 ± 0.86	19.51 ± 0.58	19.15 ± 0.6
S3 to end of section	Mediterranean	10.61 ± 1.66	15.88 ± 1.56	16.03 ± 2.2

component (~21 mT) has a pedogenic origin and its formation is favoured during interglacial periods. The second coercivity component (~50 mT) is of aeolian origin, being dominant in loess layers and with very low contribution in palaeosols.

(4) High field remanence measurements show that the hematite contribution is enhanced in palaeosols, indicating a pedogenic origin. It is also present in loess where it is probably mainly of aeolian origin. In addition, the hematite contribution depends on the degree of pedogenesis: the highest values of the hematite signal can be found in the S3, S4 and S5 palaeosols both at Mircea Vodă and Costinești. This implies that these palaeosols were formed under warmer and dryer conditions than the soils formed later. Our data from Mircea Vodă shows that high field magnetic measurements produced results similar to DRS and Munsell color based measurements.

(5) The goethite contribution, reflected by high field magnetic remanence measurements, is probably minor and constant both in loess and palaeosols.

(6) The correlation between loess sections from the Lower Danube Basin have shown that the chronology of the loess sections from the southern Ukraine and Moldavia must be revised to fit the accepted chronology of the other loess sections from this region. This revision must be extended to other loess sections from the southeastern Ukraine and the Black Sea area in order to facilitate the interpretation of climatic connections with the Danube basin region.

(7) This correlation also shows that the magnetic susceptibility data from Costinești can be interpreted as support for the transition of a Mediterranean type climate to a steppe type climate in the last two interglacial periods in the western Black Sea. Because the pattern of magnetic susceptibility data from the lower Danube basin is changing relative fast with distance from the Black Sea shore, it probably reflect the local influence of the Black Sea on continental scale climatic oscillations during the last 600 ka. The values of background magnetic susceptibility of the Romanian loess-palaeosol sections indicate a change in the dominant source area of the dust during the transition of a Mediterranean type climate to a steppe type climate.

ACKNOWLEDGEMENTS

DD was supported by the project POSDRU/159/1.5/S/133391. This research was funded by CNCS - UEFISCDI Grant PCCE_ID 31/2010. The paper was greatly improved by the comments and suggestions of the reviewers (Diana Jordanova, Christian Zeeden and an anonymous reviewer) and the editor Eduard Petrovsky.

REFERENCES

Avramov, V.I., Jordanova, D., Hoffmann, V. & Roesler, W., 2006. The role of dust source area and pedogenesis in three loess-palaeosol sections from north Bulgaria: a mineral magnetic study, *Stud. Geophys. Geod.*, **50**, 259–282.

- Balescu, S., Lamothe, M., Mercier, N., Huot, S., Balteanu, D., Billard, A. & Hus, J., 2003. Luminescence chronology of Pleistocene loess deposits from Romania: testing methods of age correction for anomalous fading in alkali feldspars, *Quat. Sci. Rev.*, **22**, 967–973.
- Balescu, S., Lamothe, M., Panaiotu, C. & Panaiotu, C., 2010. La Chronologie IRSL des sequences loessiques de l'est de la Roumanie, *Quaternaire*, **21**(2), 115–126.
- Bloemendal, J., King, J.W., Hall, F.R. & Doh, S.J., 1992. Rock magnetism of Late Neogene and Pleistocene deep-sea sediments: relationship to sediment source, diagenetic processes and sediment lithology, *J. geophys. Res.*, **97**, 4361–4375.
- Buggle, B., Glaser, B., Zoeller, L., Hambach, U., Markovic, S., Glaser, I. & Gerasimenko, N., 2008. Geochemical characterization and origin of Southeastern and Eastern European loesses (Serbia, Romania, Ukraine), *Quat. Sci. Rev.*, **27**, 1058–1075.
- Buggle, B., Hambach, U., Glaser, B., Gerasimenko, N., Marković, S.B., Glaser, I. & Zöller, L., 2009. Stratigraphy and spatial and temporal paleoclimatic trends in East European loess paleosol sequences, *Quat. Int.*, **196**, 86–106.
- Buggle, B., Hambach, U., Kehl, M., Marković, S.B., Zöller, L. & Glaser, B., 2013. The progressive evolution of a continental climate in southeast-central European lowlands during the Middle Pleistocene recorded in loess paleosol sequences, *Geology*, **41**(7), 771–774.
- Buggle, B., Hambach, U., Müller, K., Zöller, L., Marković, S.B. & Glaser, B., 2014. Iron mineralogical proxies and Quaternary climate change in SE-European loess-paleosol sequences, *Catena*, **117**, 4–22.
- Chen, T., Xie, Q., Xu, H., Chen, J., Ji, J., Lu, H. & Balsam, W., 2010. Characteristics and formation mechanism of pedogenic hematite in Quaternary Chinese loess and paleosols, *Catena*, **81**, 217–225.
- Chen, T., Qiang, X., Zhao, H. & Sun, Y., 2014. An investigation of the magnetic carriers and demagnetization characteristics of the Gulang loess section, northwestern Chinese Loess Plateau, *Geochem. Geophys. Geosyst.*, **15**, 1600–1616.
- Conea, 1970. *Quaternary Deposits from Dobrogea* (in Romanian with English abstract), Editura Academiei.
- Constantin, D., Begy, R., Vasiliu, S., Panaiotu, C., Necula, C., Codrea, V. & Timar-Gabor, A., 2014. High-resolution OSL dating of the Costinești section (Dobrogea, SE Romania) using fine and coarse quartz, *Quat. Int.*, **334–335**, 20–29.
- Cornell, R. & Schwertmann, U., 2003. *The Iron Oxide: Structure, Properties, Reactions, Occurrence, and Use*, VCH Verlagsgesellschaft.
- Day, R., Fuller, M. & Schmidt, V.A., 1977. Hysteresis properties of titanomagnetites: grain-size and compositional dependence, *Phys. Earth planet. Inter.*, **13**, 260–267.
- Dearing, J.A., Dann, R.J.L., Hay, K., Lees, J.A., Loveland, P.J., Maher, B.A. & O'Grady, K., 1996. Frequency-dependent susceptibility measurements of environmental materials, *Geophys. J. Int.*, **124**, 228–240.
- Dearing, J.A., Bird, P.M., Dann, R.J.L. & Benjamin, S.F., 1997. Secondary ferromagnetic minerals in Welsh soils: a comparison of mineral magnetic detection methods and implications for mineral formation, *Geophys. J. Int.*, **130**, 727–736.
- Dekkers, M.J., 1989. Magnetic properties of natural goethite—I. Grain-size dependence of some low- and high-field related rock magnetic parameters measured at room temperature, *Geophys. J.*, **97**, 323–340.
- Deng, C.L., 2008. Paleomagnetic and mineral magnetic investigation of the Baicaoyuan loess-paleosol sequence of the western Chinese Loess Plateau over the last glacial-interglacial cycle and its geological implication, *Geochem. Geophys. Geosyst.*, **9**(4), Q04034, doi:10.1029/2007GC001928.

- Deng, C., Zhu, R., Verosub, K.L., Singer, M.J. & Vidic, N.J., 2004. Mineral magnetic properties of loess/paleosol couplets of the central loess plateau of China over the last 1.2 Myr, *J. geophys. Res.*, **109**, B01103, doi:10.1029/2003JB002532.
- Deng, C., Vidic, N.J., Verosub, K.L., Singer, M.J., Liu, Q., Shaw, J. & Zhu, R., 2005. Mineral magnetic variation of the Jiaodao Chinese loess/paleosol sequence and its bearing on long-term climatic variability, *J. geophys. Res.*, **110**, B03103, doi:10.1029/2004JB003451.
- Deng, C.L., Shaw, J., Liu, Q.S., Pan, Y.X. & Zhu, R.X., 2006. Mineral magnetic variation of the Jingbian loess/paleosol sequence in the northern Loess Plateau of China: implications for Quaternary development of Asian aridification and cooling, *Earth planet. Sci. Lett.*, **241**(1–2), 248–259.
- Dodonov, A.E., Zhou, L.P., Markova, A.K., Tchepalyga, A.L., Trubikhin, V.M., Aleksandrovski, A.L. & Simakov, A.N., 2006. Middle–Upper Pleistocene bio-climatic and magnetic records of the Northern Black Sea Coastal Area, *Quat. Int.*, **149**(1), 44–54.
- Dunlop, D.J., 2002a. Theory and application of the Day plot (Mrs/Ms versus Hcr/Hc) 1. Theoretical curves and tests using titanomagnetite data, *J. geophys. Res.*, **107**(B3), 2056, doi:10.1029/2001JB000486.
- Dunlop, D.J., 2002b. Theory and application of the Day plot (Mrs/Ms vs. Hcr/Hc), 2. Application to data for rocks, sediments and soils, *J. geophys. Res.*, **107**(B3), 2057, doi:10.1029/2001JB000487.
- Dunlop, D.J. & Carter-Stiglitz, B., 2006. Day plots of mixtures of superparamagnetic, single-domain, pseudosingle-domain, and multidomain magnetites, *J. geophys. Res.*, **111**(B12), S09, doi:10.1029/2006JB004499.
- Dunlop, D.J. & Özdemir, Ö., 1997. *Rock Magnetism: Fundamentals and Frontiers*, Cambridge Univ. Press.
- Egli, R., 2013. VARIFORC: an optimized protocol for calculating non-regular first-order reversal curve (FORC) diagrams, *Global Planet. Change*, **110**, 302–320.
- Egli, R., Chen, A.P., Winklhofer, M., Kodama, K.P. & Horg, C.S., 2010. Detection of noninteracting single domain particles using first-order reversal curve diagrams, *Geochem. Geophys. Geosyst.*, **11**, Q01Z11, doi:10.1029/2009GC002916.
- Evans, M.E. & Heller, F., 1994. Magnetic enhancement and palaeoclimate: study of a loess/paleosol couplet across the Loess Plateau of China, *Geophys. J. Int.*, **117**, 257–264.
- Evans, M.E. & Heller, F., 2003. *Environmental Magnetism. Principles and Applications of Enviromagnetics*, Academic Press.
- Eyre, J.K., 1997. Frequency-dependence of magnetic susceptibility for populations of single domain grains, *Geophys. J. Int.*, **129**, 209–211.
- Fitzsimmons, K.E., Marković, S.B. & Hambach, U., 2012. Pleistocene environmental dynamics recorded in the loess of the middle and lower Danube basin, *Quat. Sci. Rev.*, **41**, 104–118.
- Forster, T., Evans, M.E. & Heller, F., 1994. The frequency dependence of low field susceptibility in loess sediments, *Geophys. J. Int.*, **118**, 636–642.
- France, D.E. & Oldfield, F., 2000. Identifying goethite and haematite from rock magnetic measurements of soils and sediments, *J. geophys. Res.*, **105**, 2781–2795.
- Frank, U. & Nowaczyk, N.R., 2008. Mineral magnetic properties of artificial samples systematically mixed from haematite and magnetite, *Geophys. J. Int.*, **175**, 449–461.
- Fukuma, K. & Torii, M., 2011. Absolute calibration of low- and high-field magnetic susceptibilities using rare earth oxides, *Geochem. Geophys. Geosyst.*, **12**, Q07Z28, doi:10.1029/2011GC003694.
- Ge, K., Williams, W., Liu, Q. & Yu, Y., 2014. Effects of the core-shell structure on the magnetic properties of partially oxidized magnetite grains: experimental and micromagnetic investigations, *Geochem. Geophys. Geosyst.*, **15**, 2021–2038.
- Geiss, C.E., Egli, R. & Zanner, C.W., 2008. Direct estimates of pedogenic magnetite as a tool to reconstruct past climates from buried soils, *J. geophys. Res.*, **113**, B11102, doi:10.1029/2008JB005669.
- Gendler, T.S., Heller, F., Tsatskin, A. & Spassov, S., DuPasquier, J. & Faus-tov, S.S., 2006. Roxolany and Novaya Etuliya—key sections in the western Black Sea area: magnetostratigraphy, rock magnetism and paleopedology, *Quat. Int.*, **152–153**, 78–93.
- Haase, D., Fink, J., Haase, G., Ruske, R., Pecs, M., Richter, H., Altermann, M. & Jäger, K.D., 2007. Loess in Europe—its spatial distribution based on a European Loess map, scale 1:2 500 000, *Quat. Sci. Rev.*, **26**, 1301–1312.
- Hao, Q., Oldfield, F., Bloemendal, J., Torrent, J. & Guo, Z., 2009. The record of changing hematite and goethite accumulation over the past 22 Myr on the Chinese Loess Plateau from magnetic measurements and diffuse reflectance spectroscopy, *J. geophys. Res.*, **114**, B12101, doi:10.1029/2009JB006604.
- Harrison, R.J. & Feinberg, J.M., 2008. FORCinel: an improved algorithm for calculating first-order reversal curve distributions using locally weighted regression smoothing, *Geochem. Geophys. Geosyst.*, **9**, Q05016, doi:10.1029/2008GC001987.
- Heller, F., 1978. Rock magnetic studies of Upper Jurassic limestones from southern Germany, *J. geophys.*, **44**, 525–543.
- Heslop, D., 2009. On the statistical analysis of the rock magnetic S-ratio, *Geophys. J. Int.*, **178**, 159–161.
- Heslop, D. & Dillon, M., 2007. Unmixing magnetic remanence curves without *a priori* knowledge, *Geophys. J. Int.*, **170**, 556–566.
- Heslop, D. & Roberts, A.P., 2013. Calculating uncertainties on predictions of palaeoprecipitation from the magnetic properties of soils, *Global Planet. Change*, **110**, 379–385.
- Heslop, D., Dekkers, M.J. & Langereis, C.G., 2002. Timing and structure of the Mid-Pleistocene Transition: records from the loess deposits of Northern China, *Palaeogeogr. Palaeoclimatol. Palaeoecol.*, **105**, 133–143.
- Hu, P.X., Liu, Q.S., Torrent, J., Barron, V. & Jin, C.S., 2013. Characterizing and quantifying iron oxides in Chinese loess/paleosols: implications for pedogenesis, *Earth planet. Sci. Lett.*, **369**, 271–283.
- Hu, P.X., Liu, Q.S., Heslop, D., Roberts, A.P. & Jin, C.S., 2015. Soil moisture balance and magnetic enhancement in loess–paleosol sequences from the Tibetan Plateau and Chinese Loess Plateau, *Earth planet. Sci. Lett.*, **409**, 120–132.
- Hunt, C.P., Banerjee, S.K., Han, J.M., Solheid, P.A., Oches, E., Sun, W.W. & Liu, T.S., 1995. Rock-magnetic proxies of climate change in the loess–paleosol sequence of the western Loess Plateau of China, *Geophys. J. Int.*, **123**, 232–244.
- Jin, C. & Liu, Q., 2011. Remagnetization mechanism and a new age model for L9 in Chinese loess, *Phys. Earth planet. Inter.*, **187**(3–4), 261–275.
- Jordanova, D. & Petersen, N., 1999. Palaeoclimatic record from a loess–soil profile in northeastern Bulgaria – II. Correlation with global climatic events during the Pleistocene, *Geophys. J. Int.*, **138**, 533–540.
- Jordanova, D., Hus, J. & Geeraerts, R., 2007. Palaeoclimatic implications of the magnetic record from loess/paleosol sequence Viatovo (NE Bulgaria), *Geophys. J. Int.*, **171**, 1036–1047.
- Jordanova, D., Hus, J., Evlogiev, J. & Geeraerts, R., 2008. Palaeomagnetism of the loess/paleosol sequence in Viatovo (NE Bulgaria) in the Danube basin, *Phys. Earth planet. Inter.*, **167**, 71–83.
- Jordanova, D., Grygar, T., Jordanova, N. & Petrov, P., 2011. Palaeoclimatic significance of Hematite/Goethite ratio in Bulgarian loess-paleosol sediments deduced by DRS and rock magnetic measurements, in *The Earth's Magnetic Interior*, pp. 399–412, eds Petrovský, E., Herrero-Bervera, E., Harinarayana, T. & Ivers, D., Springer.
- Lisiecki, L.E. & Raymo, M.E., 2005. A Pliocene–Pleistocene stack of 57 globally distributed benthic $\delta^{18}O$ records, *Paleoceanography*, **20**, PA1003, doi:10.1029/2004PA001071.
- Liu, Q., Banerjee, S.K., Jackson, M.J., Maher, B.A., Pan, Y., Zhu, R., Deng, C. & Chen, F., 2004a. Grain sizes of susceptibility and anhysteretic remanent magnetization carriers in Chinese loess/paleosol sequences, *J. geophys. Res.*, **109**, B03101, doi:10.1029/2003JB002747.
- Liu, Q., Banerjee, S.K., Jackson, M.J., Deng, C., Pan, Y. & Zhu, R., 2004b. New insights into partial oxidation model of magnetites and thermal alteration of magnetic mineralogy of the Chinese loess in air, *Geophys. J. Int.*, **158**(2), 506–514.
- Liu, Q.S., Banerjee, S.K., Jackson, M.J., Chen, F., Pan, Y.X. & Zhu, R.X., 2004c. Determining the climatic boundary between the Chinese loess and paleosol. Evidence from aeolian coarsegrained magnetite, *Geophys. J. Int.*, **156**, 267–274.

- Liu, Q., Roberts, A.P., Torrent, J., Horng, C.-S. & Larrasoana, J.C., 2007a. What do the HIRM and S-ratio really measure in environmental magnetism?, *Geochem. Geophys. Geosyst.*, **8**, doi:10.1029/2007GC001717.
- Liu, Q.S., Deng, C.L., Torrent, J. & Zhu, R.X., 2007b. Review of recent developments in mineral magnetism of the Chinese loess, *Quat. Sci. Rev.*, **26**, 368–385.
- Lukic, T. *et al.*, 2014. A joined rock magnetic and colorimetric perspective on the Late Pleistocene climate of Orlovat loess site (Northern Serbia), *Quat. Int.*, **334–335**, 179–188.
- Maher, B.A., 1988. Magnetic properties of some synthetic sub-micron magnetites, *J. geophys. Res.*, **94**, 83–96.
- Maher, B.A. & Taylor, R.M., 1988. Formation of ultrafine-grained magnetite in soils, *Nature*, **336**, 368–370.
- Maher, B.A. & Thompson, R., 1991. Mineral magnetic record of the Chinese loess and paleosols, *Geology*, **19**, 3–6.
- Maher, B.A. & Thompson, R., 1999. *Quaternary Climates, Environments and Magnetism*, Cambridge Univ. Press.
- Maher, B.A., Karloukovski, V.V. & Mutch, T.J., 2004. High-field remanence properties of synthetic and natural submicrometre hematites and goethites: significance for environmental contexts, *Earth planet. Sci. Lett.*, **226**, 491–505.
- Marković, S.B. *et al.*, 2009. Middle and Late Pleistocene loess sequences at Batajnica, Vojvodina, Serbia, *Quat. Int.*, **198**, 255–266.
- Marković, S.B. *et al.*, 2011. The last million years recorded at the Stari Slankamen loess paleosol sequence: revised chronostratigraphy and long-term environmental trends, *Quat. Sci. Rev.*, **30**, 1142–1154.
- Marković, S.B. *et al.*, 2012. Loess in the Vojvodina region (Northern Serbia): an essential link between European and Asian Pleistocene environments, *Netherlands J. Geosci.*, **91**(1–2), 173–188.
- Nawrocki, J., Bakhmutov, V., Bogucki, A. & Dolechi, L., 1999. The paleo-petromagnetic record in the Polish and Ukrainian loess-paleosol sequences, *Phys. Chem. Earth*, **24**(9), 773–777.
- Nawrocki, J., Bogucki, A., Lanczont, M. & Nowaczyk, N.R., 2002. The Matuyama-Brunhes boundary and the nature of magnetic remanence acquisition in the loess-paleosol sequence from western part of the East European loess province, *Palaeogeogr., Paleoclimatol., Palaeoecol.*, **188**, 39–50.
- Nawrocki, J., Lanczont, M., Rosowiecka, O. & Bogucki, A.B., 2015. Magnetostratigraphy of the loess-paleosol key Palaeolithic section at Korolevo (Transcarpathia, W Ukraine), *Quat. Int.*, doi:10.1016/j.quaint.2014.12.063.
- Necula, C. & Panaiotu, C., 2008. Application of dynamic programming to the dating of a loess-paleosol sequence, *Rom. Rep. Phys.*, **60**(1), 157–171.
- Necula, C., Panaiotu, C., Heslop, D. & Dimofte, D., 2013. Climatic control of magnetic granulometry in the Mircea Voda loess/paleosol sequence (Dobrogea, Romania), *Quat. Int.*, **293**, 5–14.
- Nie, J., Zhang, R., Necula, C., Heslop, D., Liu, Q., Gong, L. & Banerjee, S., 2014. Late Miocene–early Pleistocene paleoclimate history of the Chinese Loess Plateau revealed by remanence unmixing, *Geophys. Res. Lett.*, **41**, 2163–2168.
- Novothy, Á., Frechen, M., Horváth, E., Wacha, L. & Rolf, C., 2011. Investigating the penultimate and last glacial cycles of the Sütto loess section (Hungary) using luminescence dating, high-resolution grain size, and magnetic susceptibility data, *Quat. Int.*, **234**, 75–85.
- Orgeira, M., Egli, R. & Compagnucci, R., 2011. A quantitative model of magnetic enhancement in loessic soils, in *The Earth's Magnetic Interior*, pp. 399–412, eds Petrovský, E., Herrero-Bervera, E., Harinarayana, T. & Ivers, D., Springer.
- Panaiotu, C.G., Panaiotu, E.C., Grama, A. & Necula, C., 2001. Paleoclimatic record from a loess-paleosol profile in Southeastern Romania, *Phys. Chem. Earth*, (A) **26**(11–12), 893–898.
- Pike, C.R., Roberts, A.P. & Verosub, K.L., 2001a. FORC diagrams and thermal relaxation effects in magnetic particles, *Geophys. J. Int.*, **145**, 721–730.
- Pike, C.R., Roberts, A.P., Dekkers, M.J. & Verosub, K.L., 2001b. An investigation of multi-domain hysteresis mechanisms using FORC diagrams, *Phys. Earth planet. Inter.*, **126**, 11–25.
- Quinton, E.E., Dahms, D.E. & Geiss, C.E., 2011. Magnetic analyses of soils from the Wind River Range, Wyoming, constrain rates and pathways of magnetic enhancement for soils from semiarid climates, *Geochem. Geophys. Geosyst.*, **12**, Q07Z30, doi:10.1029/2011GC003728.
- Rădan, S.-C., 2012. Towards a synopsis of dating the loess from the Romanian plain and Dobrogea: authors and methods through time, *Geo-ECCO-Marina*, **18**, 153–171.
- Roberts, A.P., Pike, C.R. & Verosub, K.L., 2000. First-order reversal curve diagrams: a new tool for characterizing the magnetic properties of natural samples, *J. geophys. Res.*, **105**, 28 461–28 475.
- Roberts, A.P., Heslop, D., Zhao, X. & Pike, C.R., 2014. Understanding fine magnetic particle systems through use of first-order reversal curve diagrams, *Rev. Geophys.*, **52**(4), 557–602.
- Rochette, P. & Fillion, P.G., 1989. Field and temperature behaviour of remanence in synthetic goethite: palaeomagnetic implications, *Geophys. Res. Lett.*, **16**, 851–854.
- Sagnotti, L., Rochette, P., Jackson, M., Vadeboin, F., Dinares-Turell, J. & Winkler, A. “Mag-Net” Science Team, 2003. Inter-laboratory calibration of low-field magnetic and anhysteretic susceptibility measurements, *Phys. Earth planet. Inter.*, **138**, 25–38.
- Smalley, I., O'Hara-Dhand, K., Wint, J., Machalet, B., Jary, Z. & Jefferson, I., 2009. Rivers and loess: the significance of long river transportation in the complex event-sequence approach to loess deposit formation, *Quat. Int.*, **198**, 7–18.
- Song, Y., Fang, X., King, J.W., Li, J., Naotou, I. & An, Z., 2014. Magnetic parameter variations in the Chaona loess/paleosol sequences in the central Chinese Loess Plateau, and their significance for the middle Pleistocene climate transition, *Quat. Res.*, **81**(3), 433–444.
- Spasov, S., Heller, F., Kretzschmar, R., Evans, M.E., Yue, L.P. & Nourgaliev, D.K., 2003. Detrital and pedogenic magnetic mineral phases in the loess/paleosol sequence at Lingtai (Central Chinese Loess Plateau), *Phys. Earth planet. Inter.*, **140**, 255–275.
- Sun, D., Bloemendal, J., Rea, D.K., Vandenberghe, J.F., Jiang, F., An, Z. & Su, R., 2002. Grain-size distribution function of polymodal sediments in hydraulic and aeolian environments, and numerical partitioning of the sedimentary components, *Sediment. Geol.*, **152**, 263–277.
- Thompson, R. & Oldfield, F., 1986. *Environmental Magnetism*, Allen & Unwin.
- Timar, A., Vandenberghe, D., Panaiotu, E.C., Panaiotu, C.G., Necula, C., Cosma, C. & van den haute, P., 2010. Optical dating of Romanian loess using fine-grained quartz, *Quat. Geochronol.*, **5**(2–3), 143–148.
- Timar-Gabor, A., Vandenberghe, D.A.G., Vasiliniuc, S., Panaiotu, C.E., Panaiotu, C.G., Dimofte, D. & Cosma, C., 2011. Optical dating of Romanian Loess a comparison between silt-sized and sand-sized quartz, *Quat. Int.*, **240**, 62–70.
- Torrent, J., Liu, Q.S., Bloemendal, J. & Barron, V., 2007. Magnetic enhancement and iron oxides in the upper Luochuan loess-paleosol sequence, Chinese Loess Plateau, *Soil Sci. Soc. Am. J.*, **71**, 1570–1578.
- Tsatskin, A., Heller, F., Hailwood, E.A., Gendler, T.S., Hus, J., Montgomery, P., Sartori, M. & Virina, E.I., 1998. Pedosedimentary division, rock magnetism and chronology of the loess/paleosol sequence at Roxolany (Ukraine), *Palaeogeogr. Paleoclimatol. Palaeoecol.*, **143**, 111–133.
- Tsatskin, A. *et al.*, 2001. A new scheme of terrestrial paleoclimate evolution during the last 1.5Ma in the western Black Sea region: integration of soil studies and loess magnetism, *Phys. Chem. Earth*, (A) **26**(11–12), 911–916.
- Tsatskin, A., Gendler, T.S. & Heller, F., 2008. Improved paleopedological reconstruction of vertic paleosols at Novaya Etuliya, moldova via integration of soil micromorphology and environmental magnetism, in *New Trends in Soil Micromorphology*, pp. 91–110, eds Kapur, S., Mermut, A. & Stoops, G., Springer-Verlag.
- van Oorschot, I.H.M., Dekkers, M.J. & Havlicek, P., 2002. Selective dissolution of magnetic iron oxides with the acid-ammonium-oxalate/ferrousiron extraction technique e II. Natural loess and paleosol samples, *Geophys. J. Int.*, **149**, 106–117.
- van Velzen, A.J. & Dekkers, M.J., 1999. Low-temperature oxidation of magnetite in loess-paleosol sequences: a correction of rock magnetic parameters, *Stud. Geophys. Geod.*, **43**, 357–375.

- Vandenbergh, J. & Nugteren, G., 2001. Rapid climatic changes recorded in loess successions, *Global Planet. Change*, **28**, 1–9.
- Vandenbergh, J., Huijzer, B., Mûcher, H. & Laan, W., 1998. Short climatic oscillations in a western European loess sequence (Kesselt, Belgium), *J. Quat. Sci.*, **13**, 471–485.
- Vasiliniuc, S., Timar-Gabor, A., Vandenbergh, D.A.G., Panaiotu, C.G., Begy, R.C.S. & Cosma, C., 2011. A high resolution optical dating study of the Mostiștea loess-palaeosol sequence (SE Romania) using sand-sized quartz, *Geochronometria*, **38**(1), 34–41.
- Vasiliniuc, Ș., Vandenbergh, D.A.G., Timar-Gabor, A., Panaiotu, C., Cosma, C. & Van den haute, P., 2012. Testing the potential of elevated temperature post-IR-IRSL signals for dating Romanian loess, *Quat. Geochronol.*, **10**, 75–80.
- Verosub, K.L. & Roberts, A.P., 1995. Environmental magnetism: past, present, and future, *J. geophys. Res.*, **100**, 2175–2192.
- Walden, J., Oldfield, F. & Smith, J.P., 1999. Environmental magnetism: a practical guide, in *Tech. Guide 6*, Quat. Res. Assoc.
- Zhang, W., Yu, L., Lu, M., Zheng, X., Ji, J., Zhou, L. & Wang, X., 2009. East Asian summer monsoon intensity inferred from iron oxide mineralogy in the Xiashu Loess in southern China, *Quat. Sci. Rev.*, **28**, 345–353.
- Zhang, W., Dong, C., Ye, L., Ma, H. & Yu, L., 2012. Magnetic properties of coastal loess on the Midao islands, northern China: implications for provenance and weathering intensity, *Palaeogeogr. Palaeoclimatol. Palaeoecol.*, **333–334**, 160–167.
- Zhao, G. *et al.*, 2013. A long-term increasing aridification and cooling trend at the Chinese Loess Plateau during the Pliocene, *Quat. Int.*, **306**, 121–128.

SUPPORTING INFORMATION

Additional Supporting Information may be found in the online version of this paper:

Figure S1. Costinești loess-palaeosol section (43°57.304'N, 28°38.428'E, Black Sea coast, Romania). Palaeosols are labelled S1–S5. The image was taken at ~50 m north of the sampling site. The outcrop is no more visible since the cliff stabilization work along the coast.

Figure S2. Panoramic view of the loess cliffs along the Black Sea shore ~2.6 km north from the Costinești site. The outcrop is no more visible since the cliff stabilization work along the coast.

Figure S3. The loess-palaeosol section (43°58.610'N 28°39.348'E) sampled for OSL (Constantin *et al.* 2014) and IRSL (Balescu *et al.* 2003) dating. The image was taken on the Black Sea coast ~2.6 km north from the Costinești site. The palaeosols are labelled S1–S6. The outcrop is no more visible since the cliff stabilization work along the coast.

Figure S4. The loess-palaeosol section from locality 2 Mai (43°46.622'N 28°34.783'E, Black Sea coast, Romania) ~20 km south from the Costinești site. Palaeosols are labelled S1–S6.

Figure S5. Mircea Vodă loess-palaeosol section (44°19.286'N 28°11.442'E, Dobrogea plateau, Romania). Palaeosols are labelled S1–S5. Note the double palaeosol S2 corresponding to MIS 7.

Figure S6. Mostiștea loess-palaeosol section (44°15.580'N 26°52.590'E, Danube plain, Romania). Palaeosols are labelled S1–S4. Note the double palaeosol S2 corresponding to MIS 7 (<http://gji.oxfordjournals.org/lookup/suppl/doi:10.1093/gji/ggv250/-/DC1>).

Please note: Oxford University Press is not responsible for the content or functionality of any supporting materials supplied by the authors. Any queries (other than missing material) should be directed to the corresponding author for the paper.